# Exact satisfaction of boundary and interface conditions in nodal-integration-based finite element methods

Yabo Jia, Jean-Baptiste Leblond, Jean-Michel Bergheau

INSTITUT DE FRANCE
Académie des sciences

# Comptes Rendus

# Mécanique

Yabo Jia, Jean-Baptiste Leblond and Jean-Michel Bergheau

**Exact satisfaction of boundary and interface conditions in nodal-integration-based finite element methods**

Volume 350 (2022), p. 57-83

<https://doi.org/10.5802/crmeca.103>



*Les* Comptes Rendus. Mécanique *sont membres du Centre Mersenne pour l'édition scientifique ouverte*
www.centre-mersenne.org

*Comptes Rendus*
*Mécanique*
**2022**, 350, p. 57-83
https://doi.org/10.5802/crmeca.103

Short paper / *Note*

# Exact satisfaction of boundary and interface conditions in nodal-integration-based finite element methods

**Yabo Jia [a], Jean-Baptiste Leblond [*, b, c] and Jean-Michel Bergheau [a]**

[a] Université de Lyon, Ecole Centrale de Lyon, LTDS, UMR 5513 CNRS, 58 rue Jean Parot, 42023 Saint-Etienne Cedex 02, France

[b] Sorbonne Université - Faculté des Sciences et Ingénierie, Institut Jean Le Rond d'Alembert, UMR 7190 CNRS, 4 place Jussieu, 75252 Paris Cedex 05, France

[c] ESI-Group, Immeuble Le Récamier, 70 rue Robert, 69458 Lyon Cedex 06, France

*E-mails:* yabo.jia@enise.fr (Y. Jia), jbl@lmm.jussieu.fr (J.-B. Leblond), jean-michel.bergheau@enise.fr (J.-M. Bergheau)

**Abstract.** In spite of some drawbacks, finite element methods based on nodal rather than Gaussian integration present major advantages, especially in the context of elastoplastic or elastoviscoplastic problems—notably the elimination of locking problems due the plastic or viscoplastic incompressibility condition, and the reduction of computation and storage requirements pertaining to internal variables. This paper investigates another potential advantage of such methods, namely the possibility to account *exactly*—instead of approximately like with Gaussian integration—for *conditions of prescribed traction on external surfaces*, and *continuity of the traction-vector across internal interfaces separating different materials*. The technique proposed is somewhat similar to that classically used to satisfy plane stress conditions in 2D elastoplastic problems: it consists, when using the constitutive law to evaluate the stresses from the strains, in adjusting the out-of-plane components of the strain, so as to enforce either identity of the traction-vector and its prescribed value on external surfaces, or identity of the traction-vectors on both sides of internal interfaces. The examples provided for both traction-free boundaries and interfaces between materials evidence the efficiency of the technique.

**Keywords.** Finite elements, Nodal integration, External boundaries, Internal interfaces, Conditions on traction-vector.

*Manuscript received 20th January 2022, accepted 28th January 2022.*

## 1. Introduction

The prime motivation for the development of *nodal-integration-based finite element methods* (NIFEMs) probably lied in "locking" problems arising from the plastic or viscoplastic incompressibility condition, frequently encountered in nonlinear simulations of structures using the standard finite element method (FEM) based on Gaussian integration. Locking, when present, is

* Corresponding author.

due to the excessive number of Gauss points where this condition is enforced implicitly (through application of the constitutive law), as compared to that of nodes where discrete degrees of freedom are defined. A number of solutions basically retaining Gaussian integration have been proposed (see the works of Arnold *et al.* [1], Hughes [2], Brezzi and Fortin [3], Bathe [4], Heuze *et al.* [5], Feulvarch *et al.* [6], among others). But all of these solutions, which involve more complex elements, exhibit drawbacks, be they the heaviness of the meshing procedure, the increase of CPU time, or both.

A more radical solution consists of *replacing Gauss points through nodes* as integration points; this is expected to definitively solve the locking issue, since the sets of points where degrees of freedom are defined on the one hand, and where the possible incompressibility condition is enforced on the other hand, are then identical. This approach no longer requires evaluating the strain components within the elements but at the nodes, through some suitable procedure to be defined. Bonet and Burton [7] developed a 4-node tetrahedral element with average nodal pressure combined with an explicit algorithm, for applications to dynamic problems; use of such an element requires nodal calculation of the sole *hydrostatic part* of the strain tensor. Dohrmann *et al.* [8] proposed an extension of Bonet and Burton's [7] work in the form of a new 4-node tetrahedral element, combined with a nodal evaluation of *all* strain components. Other similar approaches were developed by Bonet *et al.* [9], Krysl and Zhu [10], Krysl and Kagey [11] and Castellazzi *et al.* [12]. Liu *et al.*'s [13] and Nguyen-Thoi *et al.*'s [14] *nodal smoothed finite element method* also relied on basically similar principles.

In fact, the concept of strain components defined at discrete points rather than over volumes is not limited to the context of finite elements, being also standard in meshless methods. Techniques have been developed by various authors to directly evaluate the integrals involved in the weak formulation of the problem from some arbitrary cloud of discretization points; for instance, Chen *et al.* [15, 16] and Elmer *et al.*'s [17] *stabilized conforming numerical integration* technique consists of (i) partitioning the domain studied into subvolumes containing one discretization point each; and (ii) defining strain components at every such point as the average of these components over the subvolume containing it. Such an approach may elegantly be combined with the FEM, by defining the subvolume containing a given node in relation to the finite elements containing it [18, 19]. A comparison, and a proof of the equivalence, of some of the techniques proposed for evaluation of nodal strains was very recently provided by Jia *et al.* [20].

In addition to representing a final solution to locking problems, NIFEMs appeared in time to exhibit other strong points, notably:

- The possibility of using (locking-free) linear triangular (in 2D) or tetrahedral (in 3D) meshes, permitting automatic meshing with standard tools available nowadays.
- Lesser computation and storage requirements pertaining to internal variables defined at integration points—as a consequence of the fact that in large meshes, the total number of nodes is in practice much lower than the total number of Gauss points.
- In the event of severe distortion of the elements, easy local remeshing avoiding any redefinition or displacement of the nodes.
- If required, easy transfer of quantities from one mesh to another, through use of nodal values of these quantities and shape-function-based interpolation.

Admittedly, NIFEMs are not free of shortcomings either:

- The strain tensor at some given node depends on the displacements at all *first-neighbor* nodes, which generates couplings between first-neighbor nodes in the famous "**B**-matrix" (with Zienkiewicz *et al.*'s [21] classical notations) connecting the strain tensor at a given point to the nodal displacements. This in turn generates couplings between

*second-neighbor* nodes in the global tangent-matrix, implying an increased bandwidth of this matrix.
- "Hourglass modes"—distinct from a rigid-body motion but nevertheless having zero elastic energy, as computed numerically—may be present in some cases.

In practice, however, the first disadvantage is largely compensated by the reduced number of integration points where the constitutive law must be applied. Also, Puso and Solberg [22] and Puso *et al.* [23] proposed a practically efficient remedy to the second shortcoming, consisting of applying slight corrections, derived from the standard FEM, to both the vector of residues and the tangent-matrix. Numerical experience shows that use of this remedy may be required or not, depending on the case considered.[1]

The purpose of this paper is to investigate a further possible advantage of NIFEMs, which was not envisaged at first: namely the possibility of accounting in an *exact manner* for (i) possible conditions of prescribed traction on some portion of the external boundary; and (ii) requirements of continuity of the traction-vector across possible internal interfaces between distinct materials. The impact of the resulting improvement in calculated stress distributions on external surfaces and material interfaces may be important in some cases, for instance if one wishes to investigate possible crack initiation on free surfaces, or propagation of cracks along interfaces.

With the classical FEM based on Gaussian integration, conditions of prescribed tractions on external surfaces and continuity across interfaces are only satisfied "on average", since they implicitly result from the weak formulation of the problem (equivalent to the principle of virtual work), involving integrals evaluated numerically with discretization points which never lie on the relevant external and internal surfaces. But with a nodal integration technique, integration points may be found on these surfaces, which paves the way to discrete satisfaction of the required conditions at these points. One may expect from there an improvement of the calculated mechanical fields, conspicuous for instance in visualizations of isostress lines.

However, even when nodes are used as integration points, the FEM is still based on the principle of virtual work which, in the absence of some special treatment, only warrants satisfaction of the required conditions in some average, not exact sense. Such a special treatment is therefore necessary to achieve the desired goal. In this work, we draw inspiration from the classical treatment of plane stress conditions in 2D elastoplastic or elastoviscoplastic problems, consisting of satisfying the requirement of zero stress in the direction normal to the surface meshed through gradual (iterative) adjustment of the normal component of the strain. This procedure of adjustment is extended here to all three out-of-plane components of the strain, so as to fulfill the three conditions required from the full stress-vector.

The paper is organized as follows:

- Section 2 first expounds the procedure proposed for external surfaces with conditions of prescribed traction, which basically amounts to some slight formal modification of the constitutive law. The accompanying modification of the local tangent-matrix is also presented.
- Section 3 similarly presents the procedure for internal interfaces between distinct materials.
- Section 4 discusses the practical implementation of the methods proposed. (This is done within the context of the SYSWELD™ finite element code developed by ESI-Group (SYSWELD [24]) where these methods have been implemented, but the discussion is of general scope).

[1] In the simulations presented here, it is not used because the results obtained do not seem to make it necessary.

- As a first illustration, Section 5 presents a numerical simulation of a complex thermomechanical problem involving a structure with a traction-free external boundary. This example makes quite conspicuous the improvement brought to the results through use of the procedure proposed.
- As a second illustration, Section 6 provides other numerical examples involving two geometrically simple, but materially inhomogeneous specimens. Very favorable conclusions on the efficiency of the procedure proposed are again reached.

## 2. Conditions of prescribed traction on external surfaces

### 2.1. *Generalities*

Although the emphasis of this paper is on FEMs using nodes as integration points (NIFEMs), the procedures proposed in order to exactly satisfy (i) conditions of prescribed tractions on external surfaces, in this section, and (ii) continuity of the traction-vector across internal interfaces, in the next section, are not specific to finite elements, and would apply equally well to meshless approaches. The only things that matter in this section are that:

(1) One is currently calculating the evolution of the elastoplastic or elastoviscoplastic structure between some discrete instants $t$ and $t+\Delta t$.

(2) The calculation is done iteratively, each iteration involving a "constitutive law" step (performed at each discretization point) and an "equilibrium" step (performed globally on the whole structure).

(3) At each iteration and at every discretization point, the total increment of strain $\Delta\boldsymbol{\epsilon}$ between times $t$ and $t+\Delta t$ is known and given; and the stress tensor $\boldsymbol{\sigma}$ at time $t+\Delta t$ is a function (generally complex and determined only numerically) of this strain increment, resulting from the constitutive law:[2]

$$\boldsymbol{\sigma} \equiv \mathbf{F}(\Delta\boldsymbol{\epsilon}) \quad \Leftrightarrow \quad \sigma_{ij} = F_{ij}(\Delta\boldsymbol{\epsilon}). \tag{1}$$

(4) The *local* or *constitutive tangent-matrix*

$$\mathbf{D}(\Delta\boldsymbol{\epsilon}) \equiv \frac{\partial \mathbf{F}}{\partial \Delta\boldsymbol{\epsilon}}(\Delta\boldsymbol{\epsilon}) \quad \Leftrightarrow \quad D_{ijk\ell}(\Delta\boldsymbol{\epsilon}) \equiv \frac{\partial F_{ij}}{\partial \Delta\epsilon_{k\ell}}(\Delta\boldsymbol{\epsilon}) \tag{2}$$

is calculated (numerically) simultaneously with the function $\mathbf{F}$.

(5) In addition the stress tensor $\boldsymbol{\sigma}$ should satisfy the condition

$$\boldsymbol{\sigma}\cdot\mathbf{n} = \mathbf{T}^{\text{prescr}}, \tag{3}$$

where $\mathbf{n}$ denotes the local unit exterior normal vector to the external surface, and $\mathbf{T}^{\text{prescr}}$ the prescribed traction-vector.[3]

[2] The notations $\boldsymbol{\sigma}$ and $\Delta\boldsymbol{\epsilon}$ in (1) suggest a geometrically linearized framework, with $\boldsymbol{\sigma}$ denoting Cauchy's stress tensor and $\Delta\boldsymbol{\epsilon}$ the increment of linearized strain. But the formalism applies equally well to a general geometrical framework within a *material Eulerian approach*, that is moving the mesh with the material and performing calculations on the current configuration; $\Delta\boldsymbol{\epsilon}$ must then be interpreted as the product of the Eulerian strain rate $\mathbf{d}$ and the time-increment $\Delta t$. The formalism does *not* apply to a general geometrical framework with a total or updated Lagrange option, because of a more tricky relationship between the Piola–Kirchhoff stress tensor and the traction-vector.

[3] In this theoretical section, the normal vector $\mathbf{n}$ is assumed to exist, that is, the external surface is supposed to be geometrically regular at the point considered. The situation becomes more complex when it comes to implementing the algorithm proposed below within some NIFEM, because as a rule, the surface nodes where this algorithm is to be applied belong to different discretized surface facets with different normal vectors. This issue will be discussed in Section 4 on the numerical implementation.

It is obvious that for an *arbitrary* strain increment $\Delta\boldsymbol{\epsilon}$, resulting from the procedure adopted to calculate the nodal strains, Equation (3) cannot be satisfied *exactly*; some adjustment of this increment is therefore necessary. The problem is the same as for the condition $\sigma_{33} = 0$ in 2D simulations with a plane stress option: in such simulations it is necessary, when applying the constitutive law, to adjust the normal component $\Delta\epsilon_{33}$ of the strain increment so as to fulfill this condition. However one difference is that here, assuming for definiteness the normal vector $\mathbf{n}$ to be parallel to the $x_3$-direction, *all three* out-of-plane components $\Delta\epsilon_{13}$, $\Delta\epsilon_{23}$, $\Delta\epsilon_{33}$ of the strain increment must be adjusted so as to satisfy the *three* conditions $\sigma_{13} = T_1^{\text{prescr}}$, $\sigma_{23} = T_2^{\text{prescr}}$, $\sigma_{33} = T_3^{\text{prescr}}$.

Another, more subtle difference is that in 2D plane stress calculations, the normal component $\Delta\epsilon_{33}$ of the strain increment is not known *a priori*, since the mesh is 2D in the plane $(x_1 x_2)$ and the normal component $u_3$ of the displacement is simply not considered: the value of $\Delta\epsilon_{33}$ only results from the constitutive law combined with the condition $\sigma_{33} = 0$. The situation is different here because with a 3D mesh, *all components* of the strain increment $\Delta\boldsymbol{\epsilon}$ are known at all points from nodal displacements. The possible adjustment of this increment at some points then leads to some corrected value $\Delta\boldsymbol{\epsilon}^{\text{corr}}$, so that *two* values of the full strain increment tensor are at hand at these points, $\Delta\boldsymbol{\epsilon}$ and $\Delta\boldsymbol{\epsilon}^{\text{corr}}$. This raises the following issue: *which value should be used every time the strain increment appears in the numerical algorithm?*

The answer to this question requires a careful scrutiny of the said algorithm. The strain increment appears at three distinct steps: (i) when one calculates it from nodal displacements; (ii) when one employs the constitutive law to obtain the stresses from it; (iii) when one applies the principle of virtual work to enforce equilibrium.[4] Now:

- When calculating the nodal strains from the nodal displacements, it is logical to determine the *original* strain increment $\Delta\boldsymbol{\epsilon}$, since this step is supposed to be of purely geometrical character and independent of the constitutive law.
- In contrast, when calculating the stresses, it is obviously necessary to determine and use the *corrected* strain increment $\Delta\boldsymbol{\epsilon}^{\text{corr}}$ in the constitutive law—otherwise condition (3) will not be satisfied exactly.
- Finally in the principle of virtual work, the choice of the *original* value of the virtual strain rate is dictated by the remark that use of the corrected value would raise at least two serious problems: (i) the field of corrected strain rates would have no reason to be geometrically compatible, the correction being calculated independently at the various discretization points; (ii) precisely because of the correction, this field would not be connected to the virtual velocity field by the correct kinematic relations.

The conclusion is that the corrected strain increment $\Delta\boldsymbol{\epsilon}^{\text{corr}}$ must be used *only when applying the constitutive law*: the correction of $\Delta\boldsymbol{\epsilon}$ then appears as a mere slight formal modification of the constitutive law, devoid of consequences on the rest of the numerical algorithm. This implies in particular that in the famous *global tangent-matrix* "$\int_\Omega \mathbf{B}^T \cdot \mathbf{D} \cdot \mathbf{B}\, \mathrm{d}\Omega$" (with Zienkiewicz *et al.*'s [21] notations), a correction ($\mathbf{D} \to \mathbf{D}^{\text{corr}}$) will be required for the local tangent-matrix, but *not* for the $\mathbf{B}$-matrix connecting the local strain or strain rate to the nodal displacements or velocities. An important consequence is that if the correction of the strain increment preserves the symmetry of the local tangent-matrix, it will also automatically preserve that of the global tangent-matrix.

[4] To be more exact, the principle of virtual work involves the *strain rate*, not the strain increment; but the issue remains of whether this strain rate must be corrected or not.

### 2.2. *Algorithm for satisfaction of conditions of prescribed traction*

Rather than considering, like above, a local frame "adapted" to the orientation of the normal to the external surface at the point considered, it is preferable to work in an arbitrary frame—in practice, the "general" one in which the numerical simulation is performed—in order to avoid cumbersome operations of change of frame from the general to the local frame and *vice versa*. We shall therefore use general tensorial notations not tied to any specific frame.

Since a correction is needed for the sole *out-of-plane* (with respect to the local tangent plane to the surface) components of the strain increment $\Delta\boldsymbol{\epsilon}$, the corrected strain increment $\Delta\boldsymbol{\epsilon}^{\text{corr}}$ must be of the form

$$\Delta\boldsymbol{\epsilon}^{\text{corr}} \equiv \Delta\boldsymbol{\epsilon} + \Delta\boldsymbol{\epsilon}', \quad \Delta\boldsymbol{\epsilon}' \equiv \tfrac{1}{2}(\boldsymbol{\varphi}\otimes\mathbf{n} + \mathbf{n}\otimes\boldsymbol{\varphi}), \tag{4}$$

where $\boldsymbol{\varphi}$ denotes some unknown vector to be determined. (In this way, if the $x_3$-direction is taken parallel to the exterior normal vector $\mathbf{n}$ to the surface, the components of the correction $\Delta\boldsymbol{\epsilon}'$ of the strain increment are $\Delta\epsilon'_{11} = \Delta\epsilon'_{22} = \Delta\epsilon'_{12} = 0$, as desired, and $\Delta\epsilon'_{13} = \varphi_1/2$, $\Delta\epsilon'_{23} = \varphi_2/2$, $\Delta\epsilon'_{33} = \varphi_3$.)

The vector $\boldsymbol{\varphi}$ must be determined so as to satisfy the condition (see (1) and (3)):

$$\begin{aligned} &\mathbf{G}(\boldsymbol{\varphi}) \equiv \boldsymbol{\sigma}^{\text{corr}}\cdot\mathbf{n} - \mathbf{T}^{\text{prescr}} = \mathbf{F}(\Delta\boldsymbol{\epsilon}^{\text{corr}})\cdot\mathbf{n} - \mathbf{T}^{\text{prescr}} = \mathbf{F}[\Delta\boldsymbol{\epsilon} + \Delta\boldsymbol{\epsilon}'(\boldsymbol{\varphi})]\cdot\mathbf{n} - \mathbf{T}^{\text{prescr}} = \mathbf{0} \\ \Leftrightarrow\quad &G_i(\boldsymbol{\varphi}) \equiv F_{ij}[\Delta\boldsymbol{\epsilon} + \Delta\boldsymbol{\epsilon}'(\boldsymbol{\varphi})]n_j - T_i^{\text{prescr}} = 0 \quad (\forall i), \end{aligned} \tag{5}$$

where $\boldsymbol{\sigma}^{\text{corr}} \equiv \mathbf{F}(\Delta\boldsymbol{\epsilon}^{\text{corr}})$ denotes the corrected stress tensor. In the case of an elastic constitutive law, Equation (5) on $\boldsymbol{\varphi}$ is linear so that its solution is easily found. For a general elastoplastic or elastoviscoplastic law, the equation is nonlinear; the easiest way to get the solution is to use a Newton method, wherein the value $\boldsymbol{\varphi}^{(n+1)}$ of $\boldsymbol{\varphi}$ at iteration $n+1$ is deduced from that at iteration $n$, $\boldsymbol{\varphi}^{(n)}$, through the relation

$$\boldsymbol{\varphi}^{(n+1)} = \boldsymbol{\varphi}^{(n)} - \mathbf{A}^{-1}(\boldsymbol{\varphi}^{(n)})\cdot\mathbf{G}(\boldsymbol{\varphi}^{(n)}). \tag{6}$$

In (6) the components of the tangent-matrix $\mathbf{A}$ of the algorithm are given by

$$\begin{aligned} A_{ik}(\boldsymbol{\varphi}) &\equiv \frac{\partial G_i}{\partial\varphi_k}(\boldsymbol{\varphi}) = \frac{\partial F_{ij}}{\partial\Delta\epsilon_{\ell m}}(\Delta\boldsymbol{\epsilon}^{\text{corr}})\frac{\partial\Delta\epsilon'_{\ell m}}{\partial\varphi_k}(\boldsymbol{\varphi})n_j = D_{ij\ell m}(\Delta\boldsymbol{\epsilon}^{\text{corr}})\cdot\frac{1}{2}(\delta_{k\ell}n_m + \delta_{km}n_\ell)n_j \\ &= \frac{1}{2}[D_{ijkm}(\Delta\boldsymbol{\epsilon}^{\text{corr}})n_j n_m + D_{ij\ell k}(\Delta\boldsymbol{\epsilon}^{\text{corr}})n_j n_\ell] = D_{ijk\ell}(\Delta\boldsymbol{\epsilon}^{\text{corr}})n_j n_\ell, \end{aligned} \tag{7}$$

where the symmetry property $D_{ijk\ell} = D_{ij\ell k}$ has been used. Thus $\mathbf{A}$ is nothing other than the *acoustic tensor*. Note that this tensor is symmetric if the local tangent-matrix $\mathbf{D}$ obeys the "major" symmetry property $D_{ijk\ell} = D_{k\ell ij}$. (This property is obeyed for all elasticity laws, and most—but not all—usual elastoplastic and elastoviscoplastic laws.)

In order for the Newton algorithm to run optimally, one must choose the initial value of $\boldsymbol{\varphi}$ as close as possible to the final solution of (5). A natural choice consists of that value satisfying this equation in elasticity, which is easily obtained by performing a preliminary iteration using for $\mathbf{F}$ the function corresponding to a purely elastic behavior. In this way, *if* the strain increment between times $t$ and $t+\Delta t$ at the point considered finally happens to be purely elastic, convergence of the algorithm is achieved with just one elastoplastic iteration in addition to the preliminary purely elastic one.

### 2.3. *Calculation of local tangent-matrix*

The corrected local tangent-matrix $\mathbf{D}^{\text{corr}}$ needed to construct the global tangent-matrix "$\int_\Omega \mathbf{B}^T\cdot\mathbf{D}^{\text{corr}}\cdot\mathbf{B}\,\mathrm{d}\Omega$" is defined through its components:

$$D^{\text{corr}}_{ijk\ell} \equiv \frac{\partial\sigma^{\text{corr}}_{ij}}{\partial\Delta\epsilon_{k\ell}}(\Delta\boldsymbol{\epsilon}). \tag{8}$$

It differs from $\mathbf{D}(\Delta\boldsymbol{\epsilon}^{\text{corr}}) = \partial\mathbf{F}/\partial\Delta\boldsymbol{\epsilon}(\Delta\boldsymbol{\epsilon}^{\text{corr}})$ because $\boldsymbol{\sigma}^{\text{corr}}$ depends on the solution $\boldsymbol{\varphi}$ of (5), which itself implicitly depends on $\Delta\boldsymbol{\epsilon}$.

The first task is therefore to calculate the derivatives of the components of $\boldsymbol{\varphi}$ with respect to those of $\Delta\boldsymbol{\epsilon}$. This may be achieved by differentiating equation (5) for the index $i$ with respect to $\Delta\epsilon_{k\ell}$, $\boldsymbol{\varphi}$ being taken equal to that value $\boldsymbol{\varphi}(\Delta\boldsymbol{\epsilon})$ satisfying the requested condition:

$$\begin{aligned} 0 &= \frac{\partial F_{ij}}{\partial\Delta\epsilon_{k\ell}}(\Delta\boldsymbol{\epsilon}^{\text{corr}})n_j + \frac{\partial F_{ij}}{\partial\Delta\epsilon_{mn}}(\Delta\boldsymbol{\epsilon}^{\text{corr}})\frac{\partial\Delta\epsilon'_{mn}}{\partial\varphi_p}(\boldsymbol{\varphi})\frac{\partial\varphi_p}{\partial\Delta\epsilon_{k\ell}}(\Delta\boldsymbol{\epsilon})n_j \\ &= D_{ijk\ell}(\Delta\boldsymbol{\epsilon}^{\text{corr}})n_j + A_{ip}(\boldsymbol{\varphi})\frac{\partial\varphi_p}{\partial\Delta\epsilon_{k\ell}}(\Delta\boldsymbol{\epsilon}). \end{aligned}$$

Thus, for fixed indices $k$ and $\ell$, the vector of components $\partial\varphi_p/\partial\Delta\epsilon_{k\ell}$ satisfies the vectorial equation $A_{ip}\partial\varphi_p/\partial\Delta\epsilon_{k\ell} = -D_{ijk\ell}\,n_j$, the solution of which is

$$\frac{\partial\varphi_p}{\partial\Delta\epsilon_{k\ell}}(\Delta\boldsymbol{\epsilon}) = -(A^{-1})_{pi}(\boldsymbol{\varphi})D_{ijk\ell}(\Delta\boldsymbol{\epsilon}^{\text{corr}})n_j. \tag{9}$$

It now becomes easy to calculate the components of the corrected local tangent-matrix $\mathbf{D}^{\text{corr}}$:

$$\begin{aligned} D^{\text{corr}}_{ijk\ell} &= \frac{\partial}{\partial\Delta\epsilon_{k\ell}}F_{ij}\{\Delta\boldsymbol{\epsilon} + \Delta\boldsymbol{\epsilon}'[\boldsymbol{\varphi}(\Delta\boldsymbol{\epsilon})]\} \\ &= D_{ijk\ell}(\Delta\boldsymbol{\epsilon}^{\text{corr}}) + D_{ijmn}(\Delta\boldsymbol{\epsilon}^{\text{corr}})\frac{\partial\Delta\epsilon'_{mn}}{\partial\varphi_p}(\boldsymbol{\varphi})\frac{\partial\varphi_p}{\partial\Delta\epsilon_{k\ell}}(\Delta\boldsymbol{\epsilon}) \\ &= D_{ijk\ell}(\Delta\boldsymbol{\epsilon}^{\text{corr}}) + D_{ijmn}(\Delta\boldsymbol{\epsilon}^{\text{corr}})\cdot\frac{1}{2}(\delta_{mp}n_n + \delta_{np}n_m)\frac{\partial\varphi_p}{\partial\Delta\epsilon_{k\ell}}(\Delta\boldsymbol{\epsilon}) \\ &= D_{ijk\ell}(\Delta\boldsymbol{\epsilon}^{\text{corr}}) + D_{ijmn}(\Delta\boldsymbol{\epsilon}^{\text{corr}})\frac{\partial\varphi_m}{\partial\Delta\epsilon_{k\ell}}(\Delta\boldsymbol{\epsilon})n_n, \end{aligned} \tag{10}$$

where the symmetry property $D_{ijmn} = D_{ijnm}$ has been used, and $\partial\varphi_m/\partial\Delta\epsilon_{k\ell}$ is given by (9) (with $m$ instead of $p$).

Equation (10) provides the most compact expression of the tensor $\mathbf{D}^{\text{corr}}$, adapted to its numerical computation; but its format does not clearly evidence its symmetry properties. A more convenient format in this respect may be obtained by substituting $\partial\varphi_m/\partial\Delta\epsilon_{k\ell}$ through its expression (9):

$$D^{\text{corr}}_{ijk\ell} = D_{ijk\ell}(\Delta\boldsymbol{\epsilon}^{\text{corr}}) - D_{ijmn}(\Delta\boldsymbol{\epsilon}^{\text{corr}})(A^{-1})_{mp}(\boldsymbol{\varphi})n_n n_q D_{pqk\ell}(\Delta\boldsymbol{\epsilon}^{\text{corr}}). \tag{11}$$

Then permutation of the pairs $(i,j)$ and $(k,\ell)$, followed by renaming of the pairs of repeated indices $(m,n)$ and $(p,q)$, yields

$$\begin{aligned} D^{\text{corr}}_{k\ell ij} &= D_{k\ell ij}(\Delta\boldsymbol{\epsilon}^{\text{corr}}) - D_{k\ell mn}(\Delta\boldsymbol{\epsilon}^{\text{corr}})(A^{-1})_{mp}(\boldsymbol{\varphi})n_n n_q D_{pqij}(\Delta\boldsymbol{\epsilon}^{\text{corr}}) \\ &= D_{k\ell ij}(\Delta\boldsymbol{\epsilon}^{\text{corr}}) - D_{k\ell pq}(\Delta\boldsymbol{\epsilon}^{\text{corr}})(A^{-1})_{pm}(\boldsymbol{\varphi})n_q n_n D_{mnij}(\Delta\boldsymbol{\epsilon}^{\text{corr}}) \\ &= D_{k\ell ij}(\Delta\boldsymbol{\epsilon}^{\text{corr}}) - D_{mnij}(\Delta\boldsymbol{\epsilon}^{\text{corr}})(A^{-1})_{pm}(\boldsymbol{\varphi})n_n n_q D_{k\ell pq}(\Delta\boldsymbol{\epsilon}^{\text{corr}}). \end{aligned}$$

Therefore, *if* $D_{ijk\ell} = D_{k\ell ij}$, then $D^{\text{corr}}_{ijk\ell} = D^{\text{corr}}_{k\ell ij}$ also (because the matrix $\mathbf{A}$ is symmetric). This means that the properties of "major symmetry" of the original and corrected local tangent-matrices $\mathbf{D}$ and $\mathbf{D}^{\text{corr}}$ are identical.

## 3. Continuity of traction-vector across internal interfaces between different materials

### 3.1. *Generalities*

The procedure proposed in this section to exactly satisfy continuity of the traction-vector across internal interfaces, just like that of Section 2 pertaining to conditions of prescribed tractions

on external surfaces, will apply to any numerical approach—based or not on finite elements—for which some integration points may be found on such interfaces. Again, the only points that matter are:

(1) Point (1) of Section 2.1, unmodified.
(2) Point (2), unmodified.
(3) Point (3), modified as follows: (3′): the integration point considered lies in two different materials denoted with upper indices $^1$ and $^2$; the stress tensors $\boldsymbol{\sigma}^1$, $\boldsymbol{\sigma}^2$ in these materials, at this point and at time $t+\Delta t$, are given functions (determined numerically) of the local strain increment $\Delta\boldsymbol{\epsilon}$:

$$\begin{cases} \boldsymbol{\sigma}^1 \equiv \mathbf{F}^1(\Delta\boldsymbol{\epsilon}) & \Leftrightarrow \quad \sigma^1_{ij} = F^1_{ij}(\Delta\boldsymbol{\epsilon}) \\ \boldsymbol{\sigma}^2 \equiv \mathbf{F}^2(\Delta\boldsymbol{\epsilon}) & \Leftrightarrow \quad \sigma^2_{ij} = F^2_{ij}(\Delta\boldsymbol{\epsilon}). \end{cases} \tag{12}$$

(4) Point (4), modified as follows: (4′): the constitutive tangent-matrices

$$\begin{aligned} \mathbf{D}^1(\Delta\boldsymbol{\epsilon}) \equiv \frac{\partial \mathbf{F}^1}{\partial \Delta\boldsymbol{\epsilon}}(\Delta\boldsymbol{\epsilon}) \quad &\Leftrightarrow \quad D^1_{ijk\ell}(\Delta\boldsymbol{\epsilon}) \equiv \frac{\partial F^1_{ij}}{\partial \Delta\epsilon_{k\ell}}(\Delta\boldsymbol{\epsilon}) \\ \mathbf{D}^2(\Delta\boldsymbol{\epsilon}) \equiv \frac{\partial \mathbf{F}^2}{\partial \Delta\boldsymbol{\epsilon}}(\Delta\boldsymbol{\epsilon}) \quad &\Leftrightarrow \quad D^2_{ijk\ell}(\Delta\boldsymbol{\epsilon}) \equiv \frac{\partial F^2_{ij}}{\partial \Delta\epsilon_{k\ell}}(\Delta\boldsymbol{\epsilon}) \end{aligned} \tag{13}$$

in the two materials, at the point considered, are calculated simultaneously with the functions $\mathbf{F}^1$ and $\mathbf{F}^2$.
(5) Point (5), modified as follows: (5′): the stress tensors $\boldsymbol{\sigma}^1$, $\boldsymbol{\sigma}^2$ in the two materials, at the point considered, should satisfy the condition

$$\boldsymbol{\sigma}^1 \cdot \mathbf{n} = \boldsymbol{\sigma}^2 \cdot \mathbf{n}, \tag{14}$$

where $\mathbf{n}$ denotes a local unit normal vector to the interface between the materials. (The orientation of this vector does not matter here.)[5]

Again, it is obvious that in order to satisfy condition (14), one must correct the out-of-plane components of the strain increment, the correction being here different in the two materials; $\Delta\boldsymbol{\epsilon}$ will therefore become $\Delta\boldsymbol{\epsilon}^{\mathrm{corr}\,1}$ and $\Delta\boldsymbol{\epsilon}^{\mathrm{corr}\,2}$ in materials $^1$ and $^2$, respectively. Again, the corrected strain increments $\Delta\boldsymbol{\epsilon}^{\mathrm{corr}\,1}$, $\Delta\boldsymbol{\epsilon}^{\mathrm{corr}\,2}$ will have to be used *only when applying the constitutive laws of the two materials*, not when evaluating the strain increment from the nodal displacements, nor when expressing virtual strain rates in terms of nodal virtual velocities in the principle of virtual work.

### 3.2. *Algorithm for satisfaction of continuity of traction-vector*

Again, corrections in materials $^1$ and $^2$ are required only for the out-of-plane components of the strain increment $\Delta\boldsymbol{\epsilon}$; thus the corrected strain increments $\Delta\boldsymbol{\epsilon}^{\mathrm{corr}\,1}$ and $\Delta\boldsymbol{\epsilon}^{\mathrm{corr}\,2}$ must be of the form

$$\begin{cases} \Delta\boldsymbol{\epsilon}^{\mathrm{corr}\,1} \equiv \Delta\boldsymbol{\epsilon} + \Delta\boldsymbol{\epsilon}'^1, & \Delta\boldsymbol{\epsilon}'^1 \equiv \frac{1}{2}(\boldsymbol{\varphi}^1 \otimes \mathbf{n} + \mathbf{n} \otimes \boldsymbol{\varphi}^1) \\ \Delta\boldsymbol{\epsilon}^{\mathrm{corr}\,2} \equiv \Delta\boldsymbol{\epsilon} + \Delta\boldsymbol{\epsilon}'^2, & \Delta\boldsymbol{\epsilon}'^2 \equiv \frac{1}{2}(\boldsymbol{\varphi}^2 \otimes \mathbf{n} + \mathbf{n} \otimes \boldsymbol{\varphi}^2), \end{cases} \tag{15}$$

where $\boldsymbol{\varphi}^1$ and $\boldsymbol{\varphi}^2$ are unknown vectors to be determined. However, unlike in the case of an external point subjected to some prescribed traction, the *overall* value $\Delta\boldsymbol{\epsilon}$ of the strain increment at the point of the interface considered should be left unchanged by the corrections of this increment in the two materials (since this point lies in the interior of the structure). This means

[5] The remark made in Section 2.1 about the definition of the normal vector applies equally well here.

that $w^1$ and $w^2$ denoting the "weights" of this point in materials $^1$ and $^2$ (appearing in the various discretized integrals of the weak formulation of the problem), the condition

$$w^1\Delta\boldsymbol{\epsilon}^{\mathrm{corr}\,1}+w^2\Delta\boldsymbol{\epsilon}^{\mathrm{corr}\,2}=\mathbf{0}\quad\Leftrightarrow\quad w^1\boldsymbol{\varphi}^1+w^2\boldsymbol{\varphi}^2=\mathbf{0} \tag{16}$$

should be obeyed. The implication is that we may use the vector $\boldsymbol{\varphi}^1$ as sole unknown, the other one $\boldsymbol{\varphi}^2$ being connected to it through the relation

$$\boldsymbol{\varphi}^2=-k\boldsymbol{\varphi}^1,\quad k\equiv\frac{w^1}{w^2}. \tag{17}$$

The vector $\boldsymbol{\varphi}^1$ must be determined so as to satisfy the condition (deriving from (12) and (14)):

$$\begin{aligned}\mathbf{H}(\boldsymbol{\varphi}^1)&\equiv\boldsymbol{\sigma}^{\mathrm{corr}\,1}\cdot\mathbf{n}-\boldsymbol{\sigma}^{\mathrm{corr}\,2}\cdot\mathbf{n}=[\mathbf{F}^1(\Delta\boldsymbol{\epsilon}^{\mathrm{corr}\,1})-\mathbf{F}^2(\Delta\boldsymbol{\epsilon}^{\mathrm{corr}\,2})]\cdot\mathbf{n}\\&=\{\mathbf{F}^1[\Delta\boldsymbol{\epsilon}+\Delta\boldsymbol{\epsilon}'^1(\boldsymbol{\varphi}^1)]-\mathbf{F}^2[\Delta\boldsymbol{\epsilon}+\Delta\boldsymbol{\epsilon}'^2(\boldsymbol{\varphi}^2(\boldsymbol{\varphi}^1))]\}\cdot\mathbf{n}=\mathbf{0}\\\Leftrightarrow\quad H_i(\boldsymbol{\varphi}^1)&\equiv\{F^1_{ij}[\Delta\boldsymbol{\epsilon}+\Delta\boldsymbol{\epsilon}'^1(\boldsymbol{\varphi}^1)]-F^2_{ij}[\Delta\boldsymbol{\epsilon}+\Delta\boldsymbol{\epsilon}'^2(\boldsymbol{\varphi}^2(\boldsymbol{\varphi}^1))]\}n_j=0\quad(\forall i),\end{aligned} \tag{18}$$

where $\boldsymbol{\sigma}^{\mathrm{corr}\,1}\equiv\mathbf{F}^1(\Delta\boldsymbol{\epsilon}^{\mathrm{corr}\,1})$ and $\boldsymbol{\sigma}^{\mathrm{corr}\,2}\equiv\mathbf{F}^2(\Delta\boldsymbol{\epsilon}^{\mathrm{corr}\,2})$ denote the corrected stress tensors in materials $^1$ and $^2$, respectively. Following the same steps as in Section 2.2, one calculates the components of the tangent-matrix $\mathbf{B}$ of a Newton algorithm aimed at solving this equation on $\boldsymbol{\varphi}^1$:

$$\begin{aligned}B_{ik}(\boldsymbol{\varphi}^1)&\equiv\frac{\partial H_i}{\partial\varphi^1_k}(\boldsymbol{\varphi}^1)=\left[\frac{\partial F^1_{ij}}{\partial\Delta\epsilon_{\ell m}}(\Delta\boldsymbol{\epsilon}^{\mathrm{corr}\,1})\frac{\partial\Delta\epsilon'^1_{\ell m}}{\partial\varphi^1_k}(\boldsymbol{\varphi}^1)-\frac{\partial F^2_{ij}}{\partial\Delta\epsilon_{\ell m}}(\Delta\boldsymbol{\epsilon}^{\mathrm{corr}\,2})\frac{\partial\Delta\epsilon'^2_{\ell m}}{\partial\varphi^1_k}(\boldsymbol{\varphi}^1)\right]n_j\\&=[D^1_{ijk\ell}(\Delta\boldsymbol{\epsilon}^{\mathrm{corr}\,1})+kD^2_{ijk\ell}(\Delta\boldsymbol{\epsilon}^{\mathrm{corr}\,2})]n_jn_\ell.\end{aligned} \tag{19}$$

Again, note that the matrix $\mathbf{B}$—a combination of the acoustic tensors of materials $^1$ and $^2$—is symmetric if the constitutive tangent-matrices $\mathbf{D}^1$, $\mathbf{D}^2$ obey the major symmetry properties $D^1_{ijk\ell}=D^1_{k\ell ij}$, $D^2_{ijk\ell}=D^2_{k\ell ij}$.

Here also, it is advisable to first perform a preliminary Newton iteration using for $\mathbf{F}^1$ and $\mathbf{F}^2$ the functions corresponding to a purely elastic behavior; then *if* the behavior between times $t$ and $t+\Delta t$ at the point considered happens to be purely elastic, convergence of the algorithm is achieved with just one additional iteration.

### 3.3. *Calculation of local tangent-matrices*

Like in Section 2.3, the first task is to calculate the derivatives of the components of $\boldsymbol{\varphi}^1$ with respect to those of $\Delta\boldsymbol{\epsilon}$, by differentiating equation (18) for the index $i$ with respect to $\Delta\epsilon_{k\ell}$:

$$\begin{aligned}0=&\frac{\partial F^1_{ij}}{\partial\Delta\epsilon_{k\ell}}(\Delta\boldsymbol{\epsilon}^{\mathrm{corr}\,1})n_j+\frac{\partial F^1_{ij}}{\partial\Delta\epsilon_{mn}}(\Delta\boldsymbol{\epsilon}^{\mathrm{corr}\,1})\frac{\partial\Delta\epsilon'^1_{mn}}{\partial\varphi^1_p}(\boldsymbol{\varphi}^1)\frac{\partial\varphi^1_p}{\partial\Delta\epsilon_{k\ell}}(\Delta\boldsymbol{\epsilon})n_j\\&-\frac{\partial F^2_{ij}}{\partial\Delta\epsilon_{k\ell}}(\Delta\boldsymbol{\epsilon}^{\mathrm{corr}\,2})n_j-\frac{\partial F^2_{ij}}{\partial\Delta\epsilon_{mn}}(\Delta\boldsymbol{\epsilon}^{\mathrm{corr}\,2})\frac{\partial\Delta\epsilon'^2_{mn}}{\partial\varphi^1_p}(\boldsymbol{\varphi}^1)\frac{\partial\varphi^1_p}{\partial\Delta\epsilon_{k\ell}}(\Delta\boldsymbol{\epsilon})n_j\\=&[D^1_{ijk\ell}(\Delta\boldsymbol{\epsilon}^{\mathrm{corr}\,1})-D^2_{ijk\ell}(\Delta\boldsymbol{\epsilon}^{\mathrm{corr}\,2})]n_j+B_{ip}(\boldsymbol{\varphi}^1)\frac{\partial\varphi^1_p}{\partial\Delta\epsilon_{k\ell}}(\Delta\boldsymbol{\epsilon}).\end{aligned}$$

For fixed $k$ and $\ell$, the solution of this equation on the vector of components $\partial\varphi^1_p/\partial\Delta\epsilon_{k\ell}$ reads

$$\frac{\partial\varphi^1_p}{\partial\Delta\epsilon_{k\ell}}(\Delta\boldsymbol{\epsilon})=(B^{-1})_{pi}(\boldsymbol{\varphi}^1)[D^2_{ijk\ell}(\Delta\boldsymbol{\epsilon}^{\mathrm{corr}\,2})-D^1_{ijk\ell}(\Delta\boldsymbol{\epsilon}^{\mathrm{corr}\,1})]n_j. \tag{20}$$

The components of the corrected local tangent-matrices $\mathbf{D}^{\mathrm{corr}\,1}$, $\mathbf{D}^{\mathrm{corr}\,2}$ of materials $^1$ and $^2$ then follow like in Section 2.3:

$$\begin{aligned} D^{\mathrm{corr}\,1}_{ijk\ell} &= \frac{\partial}{\partial\Delta\epsilon_{k\ell}} F^1_{ij}\{\Delta\boldsymbol{\epsilon} + \Delta\boldsymbol{\epsilon}'^1[\boldsymbol{\varphi}^1(\Delta\boldsymbol{\epsilon})]\} \\ &= D^1_{ijk\ell}(\Delta\boldsymbol{\epsilon}^{\mathrm{corr}\,1}) + D^1_{ijmn}(\Delta\boldsymbol{\epsilon}^{\mathrm{corr}\,1}) \frac{\partial\Delta\epsilon'^1_{mn}}{\partial\varphi^1_p}(\boldsymbol{\varphi}^1) \frac{\partial\varphi^1_p}{\partial\Delta\epsilon_{k\ell}}(\Delta\boldsymbol{\epsilon}) \\ &= D^1_{ijk\ell}(\Delta\boldsymbol{\epsilon}^{\mathrm{corr}\,1}) + D^1_{ijmn}(\Delta\boldsymbol{\epsilon}^{\mathrm{corr}\,1}) \frac{\partial\varphi^1_m}{\partial\Delta\epsilon_{k\ell}}(\Delta\boldsymbol{\epsilon}) n_n; \end{aligned} \tag{21}$$

$$\begin{aligned} D^{\mathrm{corr}\,2}_{ijk\ell} &= \frac{\partial}{\partial\Delta\epsilon_{k\ell}} F^2_{ij}\{\Delta\boldsymbol{\epsilon} + \Delta\boldsymbol{\epsilon}'^2[\boldsymbol{\varphi}^1(\Delta\boldsymbol{\epsilon})]\} \\ &= D^2_{ijk\ell}(\Delta\boldsymbol{\epsilon}^{\mathrm{corr}\,2}) + D^2_{ijmn}(\Delta\boldsymbol{\epsilon}^{\mathrm{corr}\,2}) \frac{\partial\Delta\epsilon'^2_{mn}}{\partial\varphi^1_p}(\boldsymbol{\varphi}^1) \frac{\partial\varphi^1_p}{\partial\Delta\epsilon_{k\ell}}(\Delta\boldsymbol{\epsilon}) \\ &= D^2_{ijk\ell}(\Delta\boldsymbol{\epsilon}^{\mathrm{corr}\,2}) - kD^2_{ijmn}(\Delta\boldsymbol{\epsilon}^{\mathrm{corr}\,2}) \frac{\partial\varphi^1_m}{\partial\Delta\epsilon_{k\ell}}(\Delta\boldsymbol{\epsilon}) n_n. \end{aligned} \tag{22}$$

The symmetry properties of $\mathbf{D}^{\mathrm{corr}\,1}$ and $\mathbf{D}^{\mathrm{corr}\,2}$ are less obvious than those of the matrix $\mathbf{D}^{\mathrm{corr}}$ of Section 2.3. To examine them, let us substitute $\partial\varphi^1_m/\partial\Delta\epsilon_{k\ell}$ through its expression (20) in (21) and (22); the results read

$$\begin{cases} D^{\mathrm{corr}\,1}_{ijk\ell} = D^1_{ijk\ell}(\Delta\boldsymbol{\epsilon}^{\mathrm{corr}\,1}) + D^1_{ijmn}(\Delta\boldsymbol{\epsilon}^{\mathrm{corr}\,1})(B^{-1})_{mp}(\boldsymbol{\varphi}^1)\, n_n n_q [D^2_{pqk\ell}(\Delta\boldsymbol{\epsilon}^{\mathrm{corr}\,2}) - D^1_{pqk\ell}(\Delta\boldsymbol{\epsilon}^{\mathrm{corr}\,1})] \\ D^{\mathrm{corr}\,2}_{ijk\ell} = D^2_{ijk\ell}(\Delta\boldsymbol{\epsilon}^{\mathrm{corr}\,2}) - kD^2_{ijmn}(\Delta\boldsymbol{\epsilon}^{\mathrm{corr}\,2})(B^{-1})_{mp}(\boldsymbol{\varphi}^1) n_n n_q [D^2_{pqk\ell}(\Delta\boldsymbol{\epsilon}^{\mathrm{corr}\,2}) - D^1_{pqk\ell}(\Delta\boldsymbol{\epsilon}^{\mathrm{corr}\,1})]. \end{cases} \tag{23}$$

Inspection of these two formulas shows that even if $\mathbf{D}^1$ and $\mathbf{D}^2$ obey the major symmetry properties $D^1_{ijk\ell} = D^1_{k\ell ij}$, $D^2_{ijk\ell} = D^2_{k\ell ij}$, neither $\mathbf{D}^{\mathrm{corr}\,1}$ nor $\mathbf{D}^{\mathrm{corr}\,2}$ does. However under such circumstances *the "overall" local tangent-matrix* $w^1\mathbf{D}^{\mathrm{corr}\,1} + w^2\mathbf{D}^{\mathrm{corr}\,2}$—the role of which will be apparent below—*does possess these symmetries*. Indeed by (23) combined with the expression $(17)_2$ of $k$,

$$\begin{aligned} w^1 D^{\mathrm{corr}\,1}_{ijk\ell} + w^2 D^{\mathrm{corr}\,2}_{ijk\ell} = {} & w^1 D^1_{ijk\ell}(\Delta\boldsymbol{\epsilon}^{\mathrm{corr}\,1}) + w^2 D^2_{ijk\ell}(\Delta\boldsymbol{\epsilon}^{\mathrm{corr}\,2}) \\ & - w^1 [D^1_{ijmn}(\Delta\boldsymbol{\epsilon}^{\mathrm{corr}\,1}) - D^2_{ijmn}(\Delta\boldsymbol{\epsilon}^{\mathrm{corr}\,2})](B^{-1})_{mp}(\boldsymbol{\varphi}^1) n_n n_q \\ & \times [D^1_{pqk\ell}(\Delta\boldsymbol{\epsilon}^{\mathrm{corr}\,1}) - D^2_{pqk\ell}(\Delta\boldsymbol{\epsilon}^{\mathrm{corr}\,2})]. \end{aligned}$$

It is then easy, following the same lines as in Section 2.3, to check that $w^1 D^{\mathrm{corr}\,1}_{ijk\ell} + w^2 D^{\mathrm{corr}\,2}_{ijk\ell} = w^1 D^{\mathrm{corr}\,1}_{k\ell ij} + w^2 D^{\mathrm{corr}\,2}_{k\ell ij}$.

## 4. Numerical implementation

We shall concentrate henceforward on FEMs using a *nodal integration scheme* (NIFEMs) and *linear tetrahedral elements*. (These are *the* elements of major interest for NIFEMs, since they permit to use standard automatic meshing tools available nowadays.)

Although the implementation of the procedures sketched in Sections 2 and 3 above, and detailed in this section, has been done in the SYSWELD™ finite element code developed by ESI-Group SYSWELD [24], and all practical examples presented in Sections 5 and 6 below have been treated with this programme, neither these procedures nor those examples involve any of its specific features: the same methods could be implemented in, and the same results obtained with, any other standard finite element code.

### 4.1. *Classification of nodes*

The procedures discussed in this paper require a clear distinction between *external* (E) nodes (belonging to some portion of the external surface subjected to some prescribed traction), *interface* (I) nodes (belonging to some internal interface between distinct materials), and all other *standard* (S) nodes. It would be awkward to force the user to define such nodes him(her)self; a reasonable extra programming effort, discussed here, permits to define these distinct categories of nodes automatically, thus avoiding to place any extra burden on the user. The procedures sketched below may be executed once and for all at the beginning of the calculation (as long as no remeshing is performed), thus minimizing their cost in CPU time.

(1) *Construction of a preliminary file*. By looping over all 3D (tetrahedral) elements, and then over the four triplets of nodes in each element, construct a provisional file (F1)—to be erased after Step 2 below—containing an ordered list of all (triangular) facets of the discretized geometry, with the following information for each facet: (i) the three numbers of the facet nodes; (ii) the number of the first element containing the facet; (iii) the number of the material this element belongs to; (iv) the number of the second element containing the facet (0 if there is no such element); (v) the number of the corresponding material (0 if the element does not exist).

(2) *Construction of external and interface facet files*. By looping over all facets in file (F1), construct two permanent files (F2) and (F3) containing ordered lists of all *external* and *interface facets*, respectively, with the following information:
   - File (F2): for every *external facet*, defined as belonging to one 3D element only: (i) the three numbers of the facet nodes $P, Q, R$, ordered in such a way that the vector product $\mathbf{PQ} \times \mathbf{PR}$ provides the orientation of the exterior normal vector to the surface; (ii) the number of the element containing the facet; (iii) the number of the corresponding material; (iv) the number of the facet as a skin (2D) element over which some traction is prescribed (0 if the facet does not exist as a skin element, that is in the absence of prescribed traction).
   - File (F3): for every *interface facet*, defined as belonging to two 3D elements lying in distinct materials: (i) the 3 numbers of the facet nodes; (ii) the number of the first element containing the facet; (iii) the number of the corresponding material; (iv) the number of the second element containing the facet;(v) the number of the corresponding material.

(3) *Beginning of construction of a node category file*. By looping over all external and interface facets in files (F2) and (F3), start the construction of a permanent file (F4) containing a list of all nodes of the structure with the following information for each node: (i) a code indicating the node type, e.g. 0 for an S node, 1 for an E node and 2 for an I node; (ii) the number of external or interface facets containing the node (0 for an S node); (iii) the numbers of these facets, according to the numberings in files (F2) and (F3); (iv) the three components of the local mean unit normal vector to the external surface or internal interface, in the initial configuration—obtained by averaging over the external or interface facets containing the node.

   Because, as will be seen, the true definition of the categories of nodes is complex and involves various special cases to be examined later, the definition adopted at this stage is only provisional. First, all nodes where at least one displacement component is prescribed are all put definitively in the S category; second, the same is done with all nodes simultaneously belonging to at least one external facet and one interface facet. (It is logical to apply a standard treatment to such nodes since no special treatment has been defined for them.) One is then left only with nodes belonging to (i) no external facet

and no interface facet; or (ii) at least one external facet but no interface facet; or (iii) no external facet but at least one interface facet. Nodes of the first type are definitively put in the S category, of the second type provisionally in the E category, of the third type provisionally in the I category.

(4) *First control of the node category file*. Looping over all nodes of type E or I in file (F4), check that for every such node, all unit normal vectors to the external or interface facets containing it are very close to each other. If they are not, put the node definitively back in the S category. (This is logical since there is then no clearly defined normal to the external surface or interface at the point considered: it is a corner- or edge-point for which no special treatment has been defined.)

(5) *Second control of the node category file*. Looping again over all nodes of type E or I in file (F4), check that: (i) for every E node, all elements containing the node are located on the "−" side of the mean unit exterior normal vector to the surface, and belong to the same material; (ii) for every I node, all elements containing the node and located on a given side, "+" or "−", of the mean unit normal vector to the interface, belong to the same material. If this condition is not satisfied, be it for an E or an I node, put the node definitively back in the S category.

The use of files (F2), (F3) and (F4) in the treatment of the constitutive law at nodes of type S, E and I will now be explained.

A final remark pertaining to the work of Weissenfels [25] is in order here. In this work the author proposed a very elegant and economical method of calculation of the "average normal vector to the boundary" at a given node. This method offers a double advantage: (i) it avoids the cumbersome determination and use of the element facets containing this node; (ii) it permits to decide automatically and very simply which nodes are located in the interior of the structure, versus on its external surface. It is regrettable that this method cannot be used in the present context, because it does not permit to compare the normal vectors to the various facets containing a given node, which is necessary to decide whether or not the normal vector to the boundary is well-defined at this point.

### 4.2. *Treatment of standard nodes*

The variational formulation of the problem results, at each time step, in a system of nonlinear equations on the nodal displacements which is solved by some iterative procedure (Newton or some variant), wherein a linear system on variations of these displacements is solved at each iteration. The left-hand side (LHS) matrix and right-hand side (RHS) vector of this system are discretized integrals over the domain considered, which are evaluated numerically by looping over all nodes of the structure, applying the constitutive law at every node to get the local stress tensor and tangent-matrix, and adding the contributions of the said node to the LHS and RHS (nodal integration). For this "summing" node, file (F4) provides the node type (S, E, I) to be considered. We first assume in this subsection that the summing node is of type S.

In such a case file (F4) is of no further use, and files (F2) and (F3) pertaining to facets are not needed at all. What is required is just standard application of the constitutive law at the summing node, circumventing use of the algorithms of Sections 2 and 3. The only difficulty is that the summing node considered, even though classified as of type S, may belong to several materials simultaneously, if it happens to have failed to pass the tests to be classified as of type I (see Section 4.1). For instance, it may belong to two materials, but with an ill-defined normal to the interface; or it may belong to three or more materials. (Recall that no special treatment has been defined for such nodes.) In such an instance one cannot unambiguously define a "stress

tensor at the node", because the said tensor is different in the various materials containing this node.

There is only one viable solution to this problem, originally proposed by Krysl and Zhu [10] in the restricted context of linear elasticity and extended here to elasto-(visco)plasticity: namely, separately calculating and storing the stress tensors and constitutive tangent-matrices *in each material containing the node considered*. This is an inevitable drawback of NIFEMs in the case of multi-material problems; it is not a serious one, however, because in practice there are not so many nodes belonging to several materials simultaneously, and the number of materials containing a given node is also limited. It is thus necessary to evaluate the nodal strain increment at the summing node, and apply the constitutive law there, separately in each material containing the node. (The nodal strain increment has no reason to be identical in the various materials.) The strain increment at the summing node in a given material is calculated from nodal increments of displacement, by looping over all elements containing the said node and belonging to this material.

Note that it is also necessary, when calculating the integrals defining the global LHS and RHS, to split them into materials. This implies a double loop, over materials and summing nodes; the ordering of the two loops is indifferent.

### 4.3. *Treatment of external nodes*

If file (F4) reveals that the summing node is of type E, a different treatment is in order. The node having passed the tests of Section 4.1 for classification as of type E, it belongs to one material only, and the external surface has a well-defined unit exterior normal vector there. All conditions are therefore gathered for use of the algorithm of Section 2, and files (F4) and (F2) provide access to the necessary data, including the value of the traction-vectors prescribed on possible skin elements containing the node. A Newton algorithm is thus superimposed upon application of the constitutive law, in order to determine the vector $\boldsymbol{\varphi}$ of (4).

Once the local corrected stress tensor $\boldsymbol{\sigma}^{\text{corr}}$ and constitutive tangent-matrix $\mathbf{D}^{\text{corr}}$ have been determined, the contributions of the summing node to the LHS and RHS may be accounted for without any additional loop on materials, since the said node belongs to a single material.

**Remark 1.** Within a geometrically linearized option (small displacement and strains), the local unit exterior normal vector to the external surface need not be re-calculated from the node positions, since it has already been calculated in the initial configuration once and for all, and made available in file (F4). In a general geometric option (large displacements and/or strains), however, it is necessary to re-calculate the present unit exterior normal vector by accounting for the present nodal displacements.

### 4.4. *Treatment of interface nodes*

Finally if, according to file (F4), the summing node is of type I, it is known—since it has passed the tests of Section 4.1 for such nodes—to belong to two materials only, unambiguously located on the two sides of an interface having a well-defined unit normal vector. Hence the algorithm of Section 3 is applicable, and files (F4) and (F3) provide the necessary data. Then the constitutive laws of the two materials are not applied in sequence but simultaneously, with a superimposed Newton algorithm aimed at determining the vector $\boldsymbol{\varphi}^1$ of (15).

Note that in such an instance the original strain increment at the summing node is *not* calculated (from nodal increments of displacement) separately in the two materials containing this node, as would be done for an S node (see Section 4.2); indeed the algorithm of Section 3

is based on use of a *single* original strain increment $\Delta\boldsymbol{\epsilon}$, shared by the two materials, at the node considered. Another seemingly viable option would be to replace this unique $\Delta\boldsymbol{\epsilon}$ through distinct original strain increments $\Delta\boldsymbol{\epsilon}^1$ and $\Delta\boldsymbol{\epsilon}^2$ in materials $^1$ and $^2$ respectively; but in addition to making the algorithm more complex, this would entail non-physical discontinuities of the in-plane components ($\Delta\epsilon_{11}$, $\Delta\epsilon_{22}$, $\Delta\epsilon_{12}$ for a normal vector parallel to the direction $x_3$) of the strain increment across the interface. With the option retained of using a single $\Delta\boldsymbol{\epsilon}$, continuity of these components across the interface is automatically ensured before the correction, and it remains so after the correction which modifies only the *out-of-plane* components of the strain increment, see (15).

Once the local corrected stress tensors $\boldsymbol{\sigma}^{\mathrm{corr}\,1}$, $\boldsymbol{\sigma}^{\mathrm{corr}\,2}$ and constitutive tangent-matrices $\mathbf{D}^{\mathrm{corr}\,1}$, $\mathbf{D}^{\mathrm{corr}\,2}$ have been calculated in materials $^1$ and $^2$ respectively, one must account for their contributions in the LHS and RHS of the global linear system. Upon nodal discretization of the relevant integrals, the contributions of the summing node to these LHS and RHS are of the form

$$w^1\,\mathbf{B}^T\cdot\boldsymbol{\sigma}^{\mathrm{corr}\,1}+w^2\,\mathbf{B}^T\cdot\boldsymbol{\sigma}^{\mathrm{corr}\,2}\quad\text{and}\quad w^1\,\mathbf{B}^T\cdot\mathbf{D}^{\mathrm{corr}\,1}\cdot\mathbf{B}+w^2\,\mathbf{B}^T\cdot\mathbf{D}^{\mathrm{corr}\,2}\cdot\mathbf{B}$$

respectively, where $w^1$ and $w^2$, like above, denote the weights of the node in the discretized integrals over materials $^1$ and $^2$, and $\mathbf{B}$ the matrix connecting the local original strain increment to the nodal increments of displacement. Now in these expressions, as another happy consequence of the use of a single original strain increment, this "$\mathbf{B}$-matrix" is the same in the terms corresponding to the two materials. Hence it may be factorized so as to put the expressions in the form

$$\mathbf{B}^T\cdot(w^1\boldsymbol{\sigma}^{\mathrm{corr}\,1}+w^2\boldsymbol{\sigma}^{\mathrm{corr}\,2})\quad\text{and}\quad\mathbf{B}^T\cdot(w^1\mathbf{D}^{\mathrm{corr}\,1}+w^2\mathbf{D}^{\mathrm{corr}\,2})\cdot\mathbf{B}.$$

This means that materials $^1$ and $^2$ may be treated as a whole, simply weighing the corresponding corrected stress tensors and constitutive tangent-matrices according to their respective weights $w^1$ and $w^2$. This implies, in particular, that the major symmetry properties (upon interchange of the first two and last two indices) of the global tangent-matrix $\int_\Omega \mathbf{B}^T\cdot\mathbf{D}\cdot\mathbf{B}\,\mathrm{d}\Omega$ depend only on those of the *overall* constitutive tangent-matrix $w^1\mathbf{D}^{\mathrm{corr}\,1}+w^2\mathbf{D}^{\mathrm{corr}\,2}$—themselves guaranteed by those of $\mathbf{D}^1$ and $\mathbf{D}^2$, see Section 3.3—and not on the (unwarranted) major symmetry properties of the *individual* tangent-matrices $\mathbf{D}^{\mathrm{corr}\,1}$ and $\mathbf{D}^{\mathrm{corr}\,2}$.

## 5. Example involving a traction-free boundary

### 5.1. *Presentation of the problem*

The problem considered pertains to a welding process performed on a plate made of SS316L stainless steel, the thermal and mechanical properties of which are provided in Appendix A. The length, width and thickness of the plate are 150 mm, 127 mm and 30 mm, respectively. A volumic heat source moves over the upper surface along a straight line located halfway across the width, at a velocity of 4 mm·s$^{-1}$; details about this source (and convective and radiative losses) are provided in Appendix B. The plate is free of mechanical constraints, except for minimal ones required to avoid rigid-body motions. The temperature-induced plastic deformations generate important residual stresses, which are to be evaluated.

Three thermomechanical computations are performed, all within a geometrically linearized option (small displacements and strains). The first is based on the classical FEM with Gaussian integration and Q1P0 elements (8-node hexahedra with continuous trilinear displacement and discontinuous constant pressure). The mesh used for this simulation, which consists of 98,578 nodes and 90,000 elements, is shown in Figure 1.

The second and third computations are based on the NIFEM depicted in Jia *et al.* [20]; the second does *not* use the special procedure of Section 2 for nodes belonging to the free surface, whereas the third does. The mesh used in both simulations, shown in Figure 2, consists of

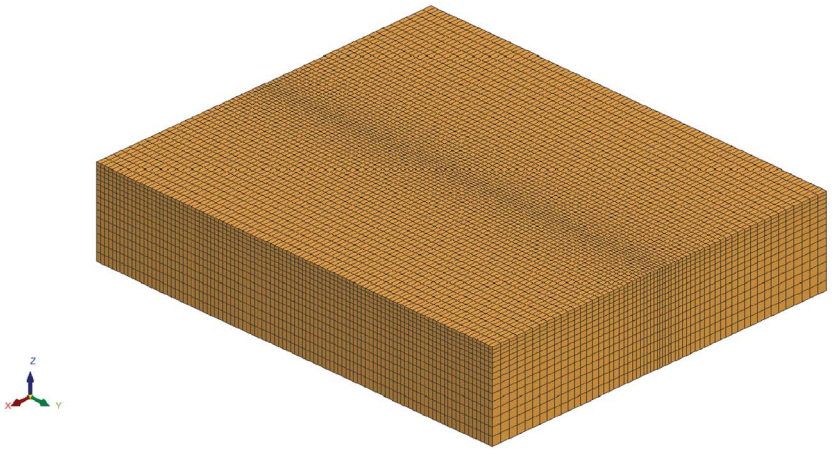

**Figure 1.** Simulation of a welding process: mesh used for the standard FEM—Gaussian integration, Q1P0 elements.

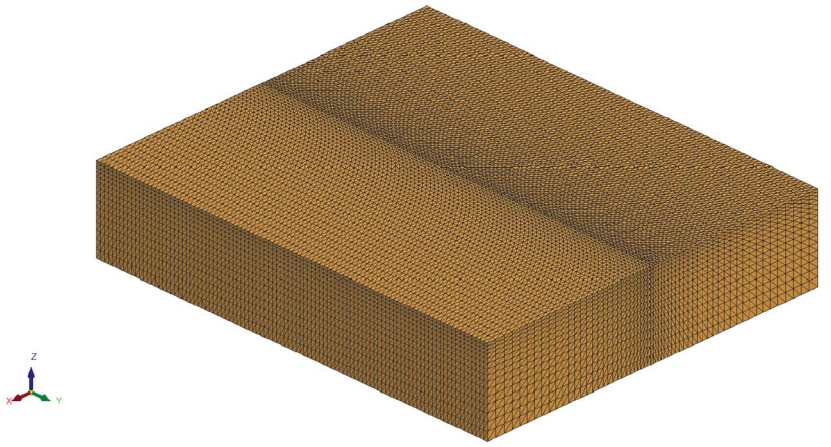

**Figure 2.** Simulation of a welding process: mesh used for the two NIFEM simulations—nodal integration, linear tetrahedral elements.

the same 98,578 nodes as in the mesh of Figure 1, but now 540,000 linear 4-node tetrahedral elements, obtained by splitting each hexahedron into six tetrahedra.

It is important to note that the Q1P0 elements of the first simulation are optimal for application of the classical FEM, since their excellent overall behavior has been noted many times. However use of such elements is easy only because of the extreme simplicity of the geometry considered (a parallelepiped). For most geometries of practical interest, meshing with such elements would only be possible manually and require much time and effort; simpler elements permitting the use of automatic meshing tools would certainly be used. This means that *the comparison between the classical FEM and the NIFEM presented here is in fact biased to some extent in favor of the former method.*

## 5.2. *Simulation results*

All numerical results presented in this subsection are provided at $t = 25$ s, at which time the center of the double ellipsoid heat source (see Appendix B) is located at $y = v_y t = 100$ mm. Figure 3

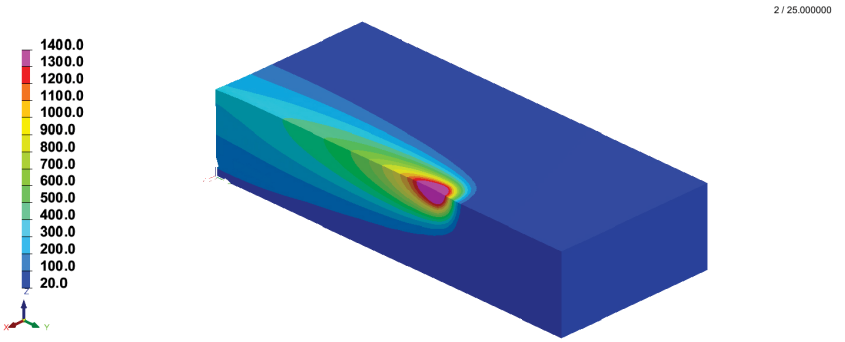


**Figure 3.** Simulation of a welding process: standard FEM simulation—distribution of temperature at time $t = 25$ s.

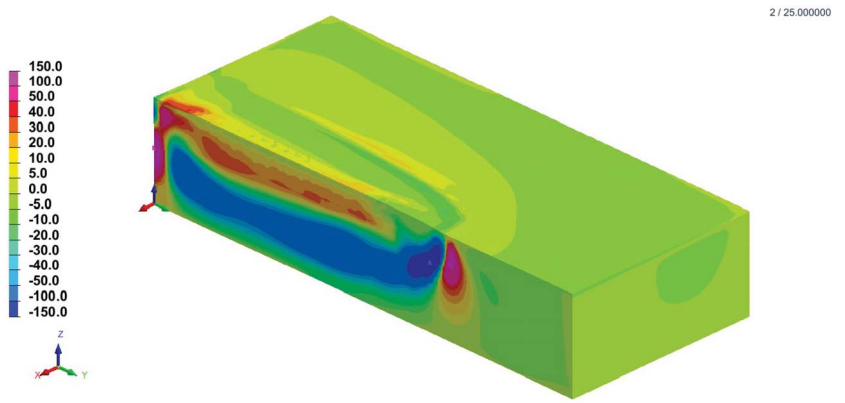


**Figure 4.** Simulation of a welding process: standard FEM simulation—distribution of vertical stress $\sigma_{zz}$ at time $t = 25$ s.

shows the temperature distribution at this instant on the surface of the plate, cut along the plane of symmetry $x = 0$ so as to permit a visualization of internal temperatures (and stresses below).[6]

Figure 4 similarly shows, for the first simulation based on the classical FEM and Q1P0 elements, the final distribution of the vertical ($\sigma_{zz}$) stress. Two points are noteworthy here. First, in spite of the relative thinness of the plate, non-negligible tensile and compressive stresses of the order of $\pm 150$ MPa are generated by the process, and the stress gradient is very high just under the moving heat source. Second, the boundary condition of zero vertical stress on the upper surface of the plate is respected only in a rough manner, this vertical stress varying between about $-10$ and $+50$ MPa.

Figure 5 provides analogous results for the second simulation based on Jia *et al.*'s [20] NIFEM with tetrahedral elements, *not* using the procedure of Section 2 for free surface nodes. The results here seem to represent an improvement over those displayed in Figure 4, in the sense that even larger stress gradients are present in the interior of the plate, meaning that such extreme gradients are better captured through nodal rather than Gaussian integration. However the boundary

[6] The temperature distributions obtained with the classical FEM and Jia *et al.*'s [20] NIFEM being almost identical, we only show here those obtained with the first method.

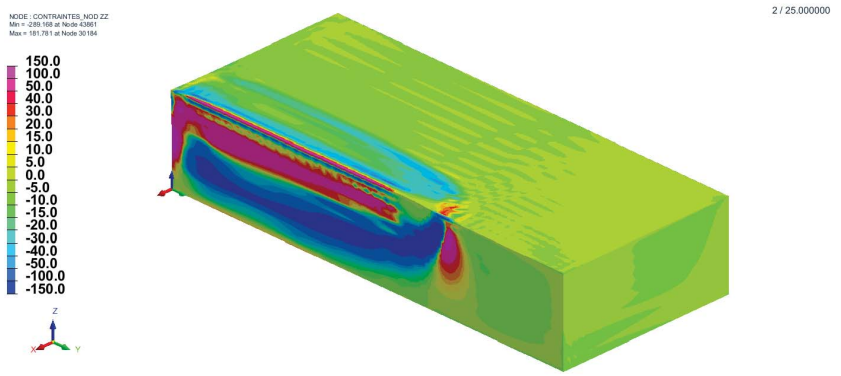


**Figure 5.** Simulation of a welding process: NIFEM simulation, no special treatment for boundary nodes—distribution of vertical stress $\sigma_{zz}$ at time $t = 25$ s.

condition of zero traction on the upper surface is poorly respected, the vertical stress varying between approximately −50 and +40 MPa.

Finally Figure 6 presents analogous results for the third simulation, identical to the second one except for the use of the procedure of Section 2 for free surface nodes; Figure 6(a) gives a general overview of isostress contours while Figure 6(b) provides additional contours for small values of $\sigma_{zz}$, thus permitting to better investigate satisfaction of the boundary condition of zero traction on the free surface. The stress distribution in the interior of the plate is quite similar to that obtained in the second simulation, but the boundary condition of zero traction on the upper surface is now very well satisfied, surface stresses being less than 1 MPa in absolute value.

The conclusion of these comparisons is thus clear: Jia *et al.*'s [20] NIFEM, used in conjunction with the procedure of Section 2 for surface nodes, permits to notably improve the results obtained with the standard FEM, with regard to satisfaction of the condition of zero traction on free surfaces. This is all the more true since, as explained above, the comparisons are biased in favor of the standard FEM.

Although the main focus of this paper is *not* on comparisons of CPU times and storage requirements in the classical FEM and Jia *et al.*'s [20] NIFEM—which have already been discussed by Jia *et al.* [20,26]—some quick remarks on the subject may be welcome. The CPU time required by the NIFEM (be it without or with the procedure of Section 2 for free surface nodes) is approximately 2.7 times larger than that required by the classical FEM (5.37 h or 5.51 h versus 2.01 h)—most probably because of the increased bandwidth of the LHS matrix in the NIFEM. On the other hand the storage needed per time step is about 8.2 smaller for the NIFEM than for the classical FEM (27.5 Mo versus 224.6 Mo)—obviously because of the reduced number of integration points in the NIFEM. Thus, as stated in the Introduction, the advantage of the NIFEM tied to the reduction of the storage requirement overcomes the drawback represented by the increase in CPU time.

## 6. Examples involving an interface between distinct materials

### 6.1. *Presentation of problems*

The problems considered here, of a more academic type, pertain to the simple tension of cylindrical specimens made of two materials, the mechanical properties of which are given in Table 1. Note that material 1 is stiffer elastically, harder plastically, and deforms less laterally, than material 2.

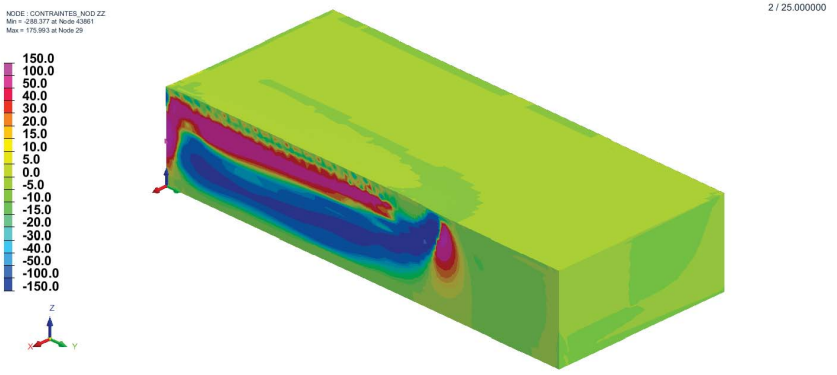


(a) Overview of isostress curves.

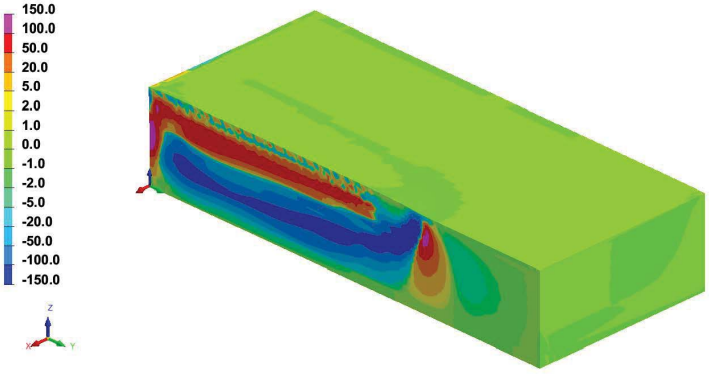


(b) Refinement near the value 0 MPa.

**Figure 6.** Simulation of a welding process: NIFEM simulation, with special treatment for boundary nodes—distribution of vertical stress $\sigma_{zz}$ at time $t = 25$ s.

**Table 1.** Mechanical constants of materials 1 and 2

| Material | $E$ (MPa) | $\nu$ | $\sigma_0$ (MPa) | Criterion | Flow rule | Hardening law |
|---|---|---|---|---|---|---|
| 1 | 200,000 | 0.2 | 500 | von Mises | Prandtl–Reuss | Ideal plasticity |
| 2 | 70,000 | 0.4 | 100 | von Mises | Prandtl–Reuss | Ideal plasticity |

The radius and height of the cylinder, of axis $Oz$, are 10 mm and 40 mm, respectively. Each material occupies half of the volume, the planar interface between the two passing through the center of the specimen, and being either perpendicular (configuration A) or parallel (configuration B) to the axis $Oz$.

Figures 7 and 8 show the meshes used for configurations A and B respectively. In each case materials 1 and 2 are painted blue and orange, respectively.

In each figure the mesh on the left is used with the classical FEM, and that on the right with Jia *et al.*'s [20] NIFEM. For configuration A, the meshes consist of: (i) for the FEM computation, 25,461 nodes and 24,800 Q1P0 elements—22,320 8-node hexahedra off the axis and 2480 6-node pentahedra (prisms of triangular basis) adjacent to it; (ii) for the NIFEM computations, the same

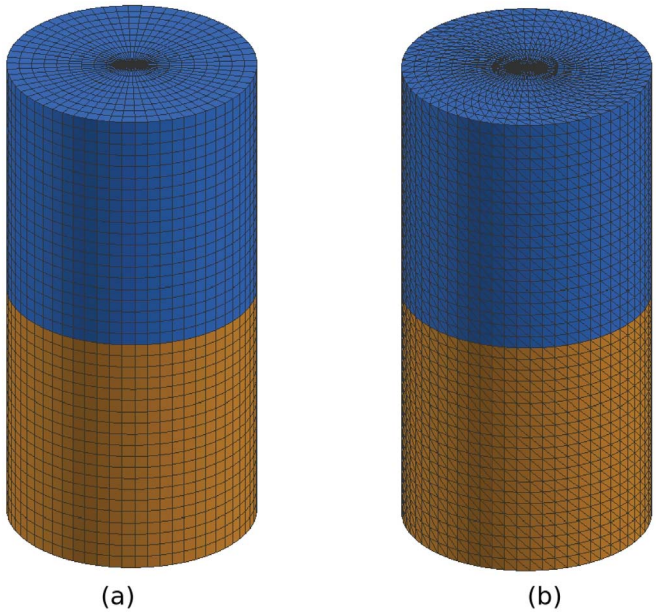


**Figure 7.** Simple tension of inhomogeneous specimen A: meshes used in the simulations based on the classical FEM (a) and the NIFEM (b).

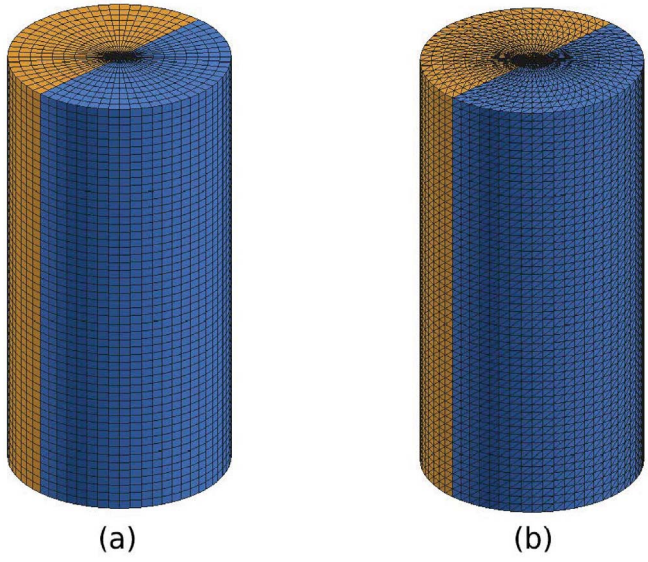


**Figure 8.** Simple tension of inhomogeneous specimen B: meshes used in the simulations based on the classical FEM (a) and the NIFEM (b).

nodes and 141,360 linear 4-node tetrahedral elements, obtained by splitting every hexahedron in the previous mesh into six tetrahedra and every pentahedron into three tetrahedra. For configuration B, the mesh used in the FEM computation similarly consists of 33,973 nodes and 33,280 elements—29,952 hexahedra and 3328 pentahedra—and the mesh used in the NIFEM computations of the same nodes and 189,696 linear tetrahedral elements.

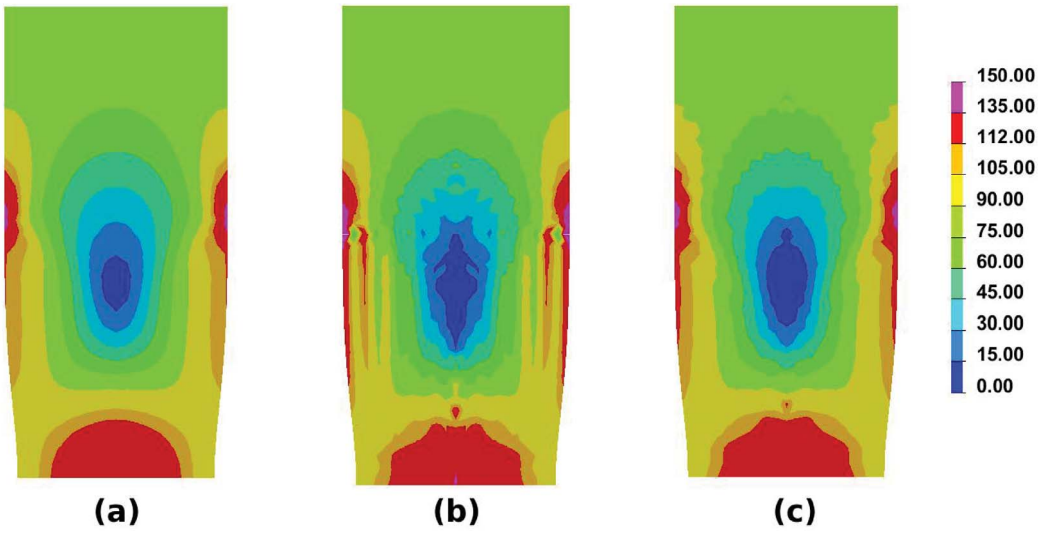


**Figure 9.** Simple tension of inhomogeneous specimen A: distribution of vertical stress $\sigma_{zz}$ for an overall axial strain of 5%—standard FEM simulation (a); NIFEM simulation, no special treatment for interface nodes (b); NIFEM simulation, with special treatment for interface nodes (c).

Unlike the computations of Section 5 performed within a geometrically linearized framework, all computations presented here are performed within a general geometrical framework (large displacements and strains), with a material Eulerian option (moving the mesh with the material and performing the calculations on the current configuration). Like before, the simulations based on Jia *et al.*'s [20] NIFEM are done both without and with the special procedure of Section 3 for nodes lying on the interface between the materials.

It is important to note again that just like in Section 5, and for the same reasons, the present comparison between the classical FEM and the NIFEM is biased in favor of the former method.

### 6.2. *Simulation results*

We consider configuration A first. Figure 9 first shows the distributions of the vertical stress $\sigma_{zz}$ obtained in the three types of simulations, at an instant corresponding to an overall axial strain of 5%, on the vertical plane $y = 0$. This stress component is theoretically supposed to be continuous across the horizontal interface between the materials.[7]

Several points are noteworthy here:

- First, in all simulations the difference between the two materials generates an important heterogeneity of the stress, which varies roughly between −10 MPa and 130 MPa.
- The stress distribution obtained with the classical FEM—diagram (a)—is nice and smooth.
- The stress distribution obtained with the NIFEM without using the procedure of Section 3 for interface nodes—diagram (b)—is approximately continuous across the interface. But

[7] Since a general geometrical framework is used, the normal unit vector $\mathbf{n}$ to the interface is considered on the current configuration and slightly differs from the unit vertical vector $\mathbf{e}_z$; but this effect is small and may safely be ignored when interpreting the figures.

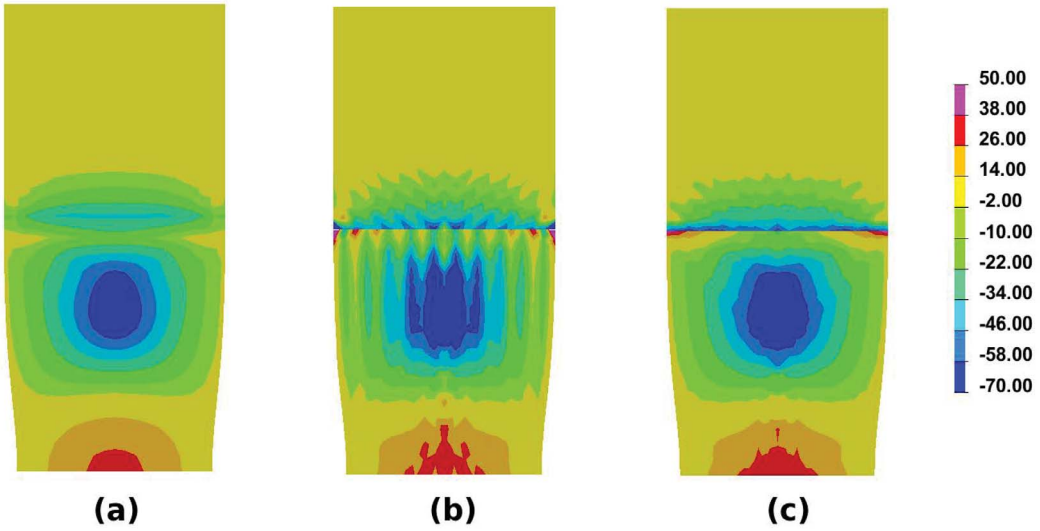


**Figure 10.** Simple tension of inhomogeneous specimen A: distribution of horizontal stress $\sigma_{xx}$ for an overall axial strain of 5%—standard FEM simulation (a); NIFEM simulation, no special treatment for interface nodes (b); NIFEM simulation, with special treatment for interface nodes (c).

it is somewhat chaotic in the vicinity of this interface, stress oscillations being observable along horizontal lines located below it, even at some distance from it.

- When use of the NIFEM is combined with that of the procedure of Section 3 for interface nodes—diagram (c)—the vertical stress is perfectly continuous across the interface and irregularities of its distribution are greatly, if not completely, reduced. (Note that the procedure for free surface nodes is activated simultaneously with that for interface nodes, so that *both* procedures are in fact responsible for the improvements.)

Figures 10 and 11 now show the distributions of the horizontal stresses $\sigma_{xx}$ and $\sigma_{yy}$, again on the vertical plane $y = 0$. These stress components have no theoretical reason to be continuous across the horizontal interface.

One may note here that:

- The stress distributions obtained with the classical FEM are again smooth, although they vary somewhat quickly in the vicinity of the interface. But since the stress components considered here are *not* expected to be continuous across the interface, this relative smoothness is no longer an advantage but rather a drawback.[8]
- In contrast, the stress distributions obtained with the NIFEM without any special treatment for interface nodes exhibit a clear discontinuity across the interface. However they are again somewhat chaotic, with stress oscillations along horizontal lines below the interface.
- The stress distributions obtained with the NIFEM using the special treatment for interface nodes of Section 3 also exhibit a clear discontinuity across the interface, but are considerably smoother below.

[8]This smoothness certainly arises at least partly from the procedure of "transfer" of the stress tensor from the Gauss points to the nodes, which precedes the drawing of the figure. But such a procedure is unfortunately unavoidable with the classical FEM based on Gaussian integration.

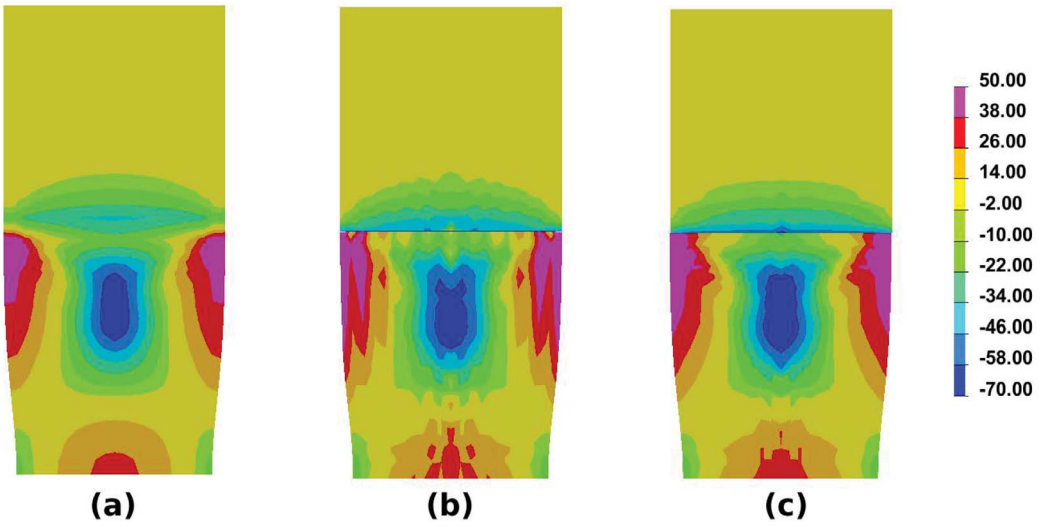


**Figure 11.** Simple tension of inhomogeneous specimen A: distribution of horizontal stress $\sigma_{yy}$ for an overall axial strain of 5%—standard FEM simulation (a); NIFEM simulation, no special treatment for interface nodes (b); NIFEM simulation, with special treatment for interface nodes (c).

An ancillary remark about Figure 10(c) is that the condition $\sigma_{xx} = 0$ is *not* satisfied as it should at the two points of intersection of the interface and the free surface (where the exterior normal vector is $\pm\mathbf{e}_x$). The explanation is that as mentioned in passing in Section 4.1, no special procedure has been developed for nodes of this (rare) type, which are thus simply treated as "standard".

We now consider configuration B of the heterogeneous specimen. The interface between the materials then coincides with the plane $y = 0$; hence the stress component $\sigma_{yy}$ should be continuous across the interface, and the components $\sigma_{xx}$ and $\sigma_{zz}$ discontinuous. Figures 12–14 show the distributions of these components (starting again with the hopefully continuous one $\sigma_{yy}$) on the vertical plane $x = 0$, for an overall axial strain of 5%.

The conclusions drawn from these figures are basically the same as for configuration A:

- The standard FEM provides good results but exaggerates the smoothness of supposedly discontinuous stress components in the vicinity of the interface.
- The NIFEM without any special treatment of interface nodes wrongly yields a slightly discontinuous $\sigma_{yy}$ component.
- The NIFEM with a special treatment of interface nodes clearly distinguishes between supposedly continuous and discontinuous stress components.

One may also note incidentally, about Figure 12, that the requested condition $\sigma_{yy} = 0$ is *not* satisfied at the lower right corner in the FEM simulation, whereas it is in both NIFEM simulations.

The general conclusion of this section is thus just as clear as that of the preceding one: use of Jia *et al.*'s [20] NIFEM, in conjunction with the procedure of Section 3 for surface nodes, leads to a notable improvement of the results obtained with the classical FEM, with regard to satisfaction of conditions of continuity across material interfaces. *The results obtained with Jia et al.'s [20] NIFEM, coupled with the procedure of Section 3, are the only ones that make a clear distinction between stress components expected to be continuous/discontinuous across material interfaces.* Again, this is all the more true since the comparisons are biased in favor of the classical FEM.

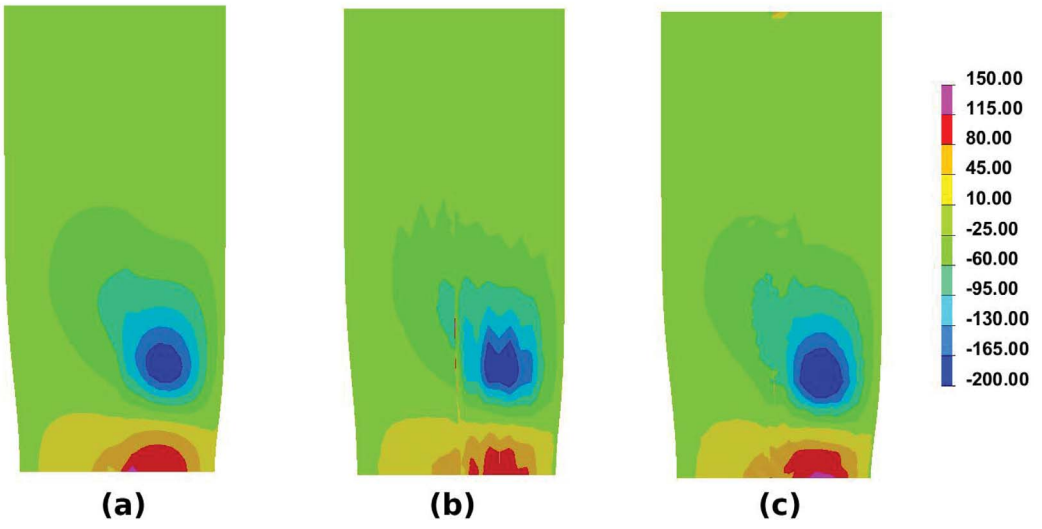


**Figure 12.** Simple tension of inhomogeneous specimen B: distribution of horizontal stress $\sigma_{yy}$ for an overall axial strain of 5%—standard FEM simulation (a); NIFEM simulation, no special treatment for interface nodes (b); NIFEM simulation, with special treatment for interface nodes (c).

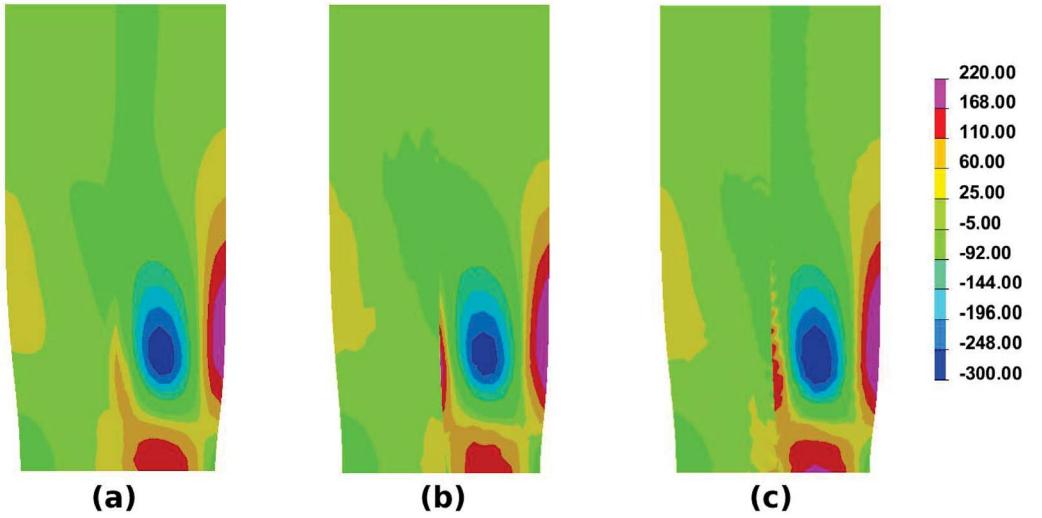


**Figure 13.** Simple tension of inhomogeneous specimen B: distribution of horizontal stress $\sigma_{xx}$ for an overall axial strain of 5%—standard FEM simulation (a); NIFEM simulation, no special treatment for interface nodes (b); NIFEM simulation, with special treatment for interface nodes (c).

## 7. Concluding synthesis

The aim of this paper was to investigate an interesting bonus of NIFEMs for deformable (elastic, elastoplastic or elastoviscoplastic) solids: namely the possibility of *exactly* accounting for (i) possible conditions of prescribed traction on external surfaces; and (ii) continuity of the traction-

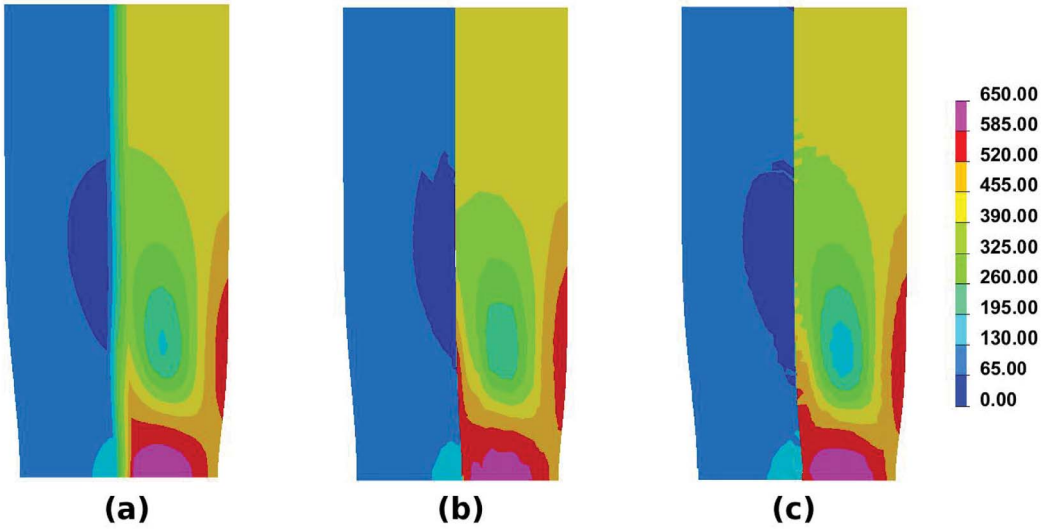


**Figure 14.** Simple tension of inhomogeneous specimen B: distribution of vertical stress $\sigma_{zz}$ for an overall axial strain of 5%—standard FEM simulation (a); NIFEM simulation, no special treatment for interface nodes (b); NIFEM simulation, with special treatment for interface nodes (c).

vector across internal interfaces between different materials. Such a possibility is important in some problems, when accurate stress distributions on external surfaces and/or material interfaces are required, for instance to investigate possible crack initiation on free surfaces or propagation of cracks along interfaces. It is ruled out in the classical FEM based on Gaussian integration, because the constitutive law is applied, and the stresses are calculated, at some internal points within the elements which never lie on external surfaces or internal interfaces.

In Section 2, we discussed a special procedure aimed at exactly respecting conditions of prescribed traction at some node located on some external surface. The principle was inspired from the classical numerical treatment of 2D plane stress problems; it consisted in correcting the three out-of-plane components of the strain calculated from the nodal displacements, so as to satisfy the said conditions. With such a procedure the strain tensor exists in two forms, original and corrected. The latter form is relevant when one uses the constitutive law to calculate the stress tensor; but the original form must be preferred when writing the principle of virtual work, in order to retain the necessary consistency of the displacement and strain fields. The procedure proposed thus formally appears as a mere slight modification of the sole constitutive law.

In Section 3, we discussed a similar procedure aimed at exactly respecting continuity of the traction-vector across internal interfaces between distinct materials. The principle was analogous to, albeit a bit more complex than, that for boundary nodes; it consisted of modifying the out-of-plane components of the strain tensors in the two materials containing the node considered—while respecting their average over these materials—so as to achieve the desired continuity. Again, the local strain tensor then exists in two forms: the corrected form must be used when applying the constitutive laws of the two materials, and the original one when applying the principle of virtual work.

Section 4 was devoted to an in-depth discussion of the numerical implementation of the algorithms proposed. The main topic in this section was a depiction of automatic procedures—aimed at sparing the user's data input effort—for: (i) classification of the nodes into three categories: "standard" (not requiring any special treatment), "external" (liable to the treatment

of Section 2), and "interface" (liable to the treatment of Section 3); (ii) calculation and storage of information pertaining to the last two categories of nodes, needed for the application of the procedures discussed previously. A briefer discussion of the numerical treatment of the various types of nodes was then provided.

In Section 5, we provided an example of application of the procedure of Section 2 to a problem involving a structure with a free external surface. This structure was geometrically simple—a plate—but subjected to some rather complex thermal loading resulting from a welding operation. Three types of calculations were performed, using (i) the standard FEM; (ii) Jia *et al.*'s [20] NIFEM without the procedure of Section 2 for free surface nodes; and (iii) the same method with this procedure. The results clearly evidenced the advantages of the last method, at no significant additional cost.

Finally Section 6 provided two examples of application of the procedure of Section 3 to problems involving simple specimens made of two materials bonded onto one another. These specimens were circular cylinders subjected to simple tension, with an interface between the materials either perpendicular or parallel to their central axis. Again, the comparisons clearly evidenced the advantage of using the NIFEM with a special treatment for interface nodes.

To conclude, it should be remarked that when defining the procedures of Sections 2 and 3, we excluded for simplicity some cases of practical interest: for instance that of a node located on some plane of symmetry of the structure, for which the normal component of the displacement and the two tangential components of the traction-vector are requested to be zero. It would not be difficult, in principle, to treat such cases through suitable extensions of the procedures presented above.

## Conflicts of interest

Authors have no conflict of interest to declare.

## Acknowledgment

The authors wish to express their sincere thanks to Professor Pierre Suquet, of Centre National de la Recherche Scientifique (CNRS), who suggested the work depicted in this paper.

## Appendix A. Material properties used in the simulations of Section 5

The thermal and mechanical properties of the SS316L stainless steel considered in Section 5 are provided in Figure 15 in graphical form. The left diagram here illustrates the variations of the thermal conductivity, mass density, specific heat, thermal strain (harmlessly truncated at 1400 °C) and Young's modulus with the temperature. (A constant value of 0.3 is adopted for Poisson's ratio.) The right diagram shows the (stress)–(plastic strain) curve in simple tension at various temperatures; plasticity is assumed to be governed by the von Mises criterion and the associated (Prandtl–Reuss) flow rule, hardening being of purely isotropic nature.

## Appendix B. Details on thermal data in the simulations of Section 5

The simulations of Section 5 consider a moving "double ellipsoid heat source" Goldak *et al.* [27] defined by the following heat inputs per unit volume (with "f" and "r" meaning "front" and "rear"):

$$\begin{cases} q_f = Q_f \exp\left(-\dfrac{(y-v_y t)^2}{a_f^2}\right)\exp\left(-\dfrac{x^2}{b^2}\right)\exp\left(-\dfrac{(z-z_0)^2}{c^2}\right) & \text{for } y > v_y t \\ q_r = Q_r \exp\left(-\dfrac{(y-v_y t)^2}{a_r^2}\right)\exp\left(-\dfrac{x^2}{b^2}\right)\exp\left(-\dfrac{(z-z_0)^2}{c^2}\right) & \text{for } y < v_y t \end{cases}$$

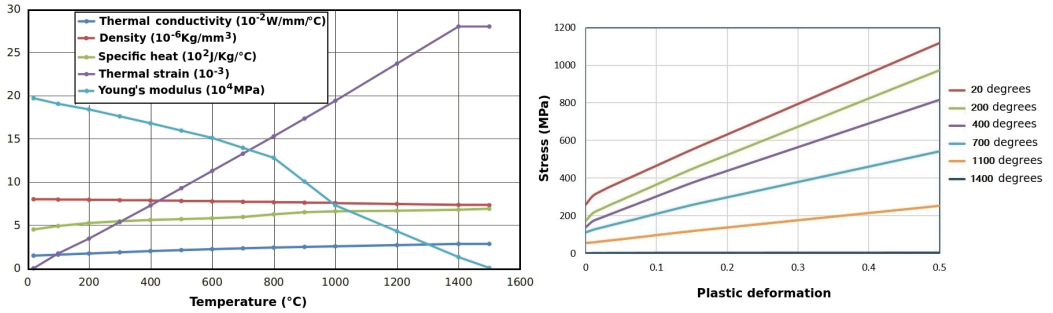


**Figure 15.** Material (thermal and mechanical) properties of the SS316L stainless steel.

with

$$\begin{cases} Q_f = 14\ \mathrm{W{\cdot}mm^{-3}}; \quad Q_r = 7.6\ \mathrm{W{\cdot}mm^{-3}} \\ a_f = 2\ \mathrm{mm}; \quad a_r = 6\ \mathrm{mm} \\ b = 6\ \mathrm{mm} \\ c = 6\ \mathrm{mm} \\ z_0 = 30\ \mathrm{mm} \\ v_y = 4\ \mathrm{mm{\cdot}s^{-1}}; \end{cases}$$

the coordinates $x, y, z$ in these expressions are specified in Figures 1 and 2.[9]

Also, thermal convective losses in the atmosphere are simulated through some heat transfer coefficient $h_{\mathrm{conv}} = 35 \times 10^{-6}\ \mathrm{W{\cdot}mm^{-2}{\cdot}(^\circ\,C)^{-1}}$; and radiative losses through some output thermal flux $J_{\mathrm{rad}} = \epsilon\sigma(T^4 - T_0^4)$ where $\epsilon = 0.8$ denotes the emissivity, $\sigma = 5.67 \times 10^{-14}\ \mathrm{W{\cdot}mm^{-2}{\cdot}K^{-4}}$ Stefan's constant, $T$ the local absolute temperature in K, and $T_0$ the room temperature of 20 °C = 293.15 K.

## References

[1] D. N. Arnold, F. Brezzi, M. Fortin, "A stable finite element for the Stokes equations", *Calcolo* **21** (1984), p. 337-344.

[2] T. J. R. Hughes, *The Finite Element Method: Linear Static and Dynamic Finite Element Analysis*, Prentice-Hall, Upper Saddle River, NJ, 1987.

[3] F. Brezzi, M. Fortin, *Mixed and Hybrid Finite Element Methods*, Springer-Verlag, New York, 1991.

[4] K. Bathe, *Finite Element Procedure*, Prentice-Hall, Upper Saddle River, NJ, 1996.

[5] T. Heuzé, H. Amin-El-Sayed, J. B. Leblond, J. M. Bergheau, "Benchmark tests based on the Couette viscometer—II: thermo-elasto-plastic solid behaviour in small and large strains", *Comput. Math. Appl.* **67** (2014), p. 1482-1496.

[6] E. Feulvarch, J. C. Roux, J. M. Bergheau, P. Gilles, "A stable P1/P1 finite element for finite strain von Mises elasto-plasticity", *Comput. Methods Appl. Mech. Eng.* **324** (2017), p. 537-545.

[7] J. Bonet, J. Burton, "A simple average nodal pressure tetrahedral element for incompressible and nearly incompressible dynamic explicit applications", *Commun. Numer. Methods Eng.* **14** (1998), p. 437-449.

[8] C. R. Dohrmann, M. W. Heinstein, J. Jung, S. W. Key, W. R. Witkowski, "Node-based uniform strain elements for three-node triangular and four-node tetrahedral meshes", *Int. J. Numer. Methods Eng.* **47** (2000), p. 1549-1568.

[9] J. Bonet, H. Marriott, O. Hassan, "An averaged nodal deformation gradient linear tetrahedral element for large strain explicit dynamic applications", *Commun. Numer. Methods Eng.* **17** (2001), p. 551-561.

[10] P. Krysl, B. Zhu, "Locking-free continuum displacement finite elements with nodal integration", *Int. J. Numer. Methods Eng.* **76** (2008), p. 1020-1043.

[11] P. Krysl, H. Kagey, "Reformulation of nodally integrated continuum elements to attain insensitivity to distortion", *Int. J. Numer. Methods Eng.* **90** (2012), p. 805-818.

[12] G. Castellazzi, E. Artioli, P. Krysl, "Linear tetrahedral element for problems of plastic deformation", *Meccanica* **50** (2015), p. 3069-3086.

[9] These parameters are chosen somewhat arbitrarily, but correspond in order of magnitude to welding by a TIG or MIG process.

[13] G. R. Liu, T. Nguyen-Thoi, H. Nguyen-Xuan, K. Y. Lam, "A node-based smoothed finite element method (NS-FEM) for upper bound solutions to solid mechanics problems", *Comput. Struct.* **87** (2009), p. 14-26.
[14] T. Nguyen-Thoi, H. C. Vu-Do, T. Rabczuk, H. Nguyen-Xuan, "A node-based smoothed finite element method (NS-FEM) for upper bound solution to visco-elastoplastic analyses of solids using triangular and tetrahedral meshes", *Comput. Methods Appl. Mech. Eng.* **199** (2010), p. 3005-3027.
[15] J. S. Chen, C. T. Wu, S. Yoon, Y. You, "A stabilized conforming nodal integration for Galerkin mesh-free methods", *Int. J. Numer. Methods Eng.* **50** (2001), p. 435-466.
[16] J. S. Chen, S. Yoon, C. T. Wu, "Non-linear version of stabilized conforming nodal integration for Galerkin mesh-free methods", *Int. J. Numer. Methods Eng.* **53** (2002), p. 2587-2615.
[17] W. Elmer, J. S. Chen, M. Puso, E. Taciroglu, "A stable, meshfree, nodal integration method for nearly incompressible solids", *Finite Elem. Anal. Des.* **51** (2012), p. 81-85.
[18] W. Quak, A. H. van den Boogaard, D. González, E. Cueto, "A comparative study on the performance of meshless approximations and their integration", *Comput. Mech.* **48** (2011), p. 121-137.
[19] D. Canales, A. Leygue, F. Chinesta, I. Alfaro, D. González, E. Cueto, E. Feulvarch, J. M. Bergheau, "In-plane/out-of-plane separated representations of updated Lagrangian descriptions of viscoplastic flow models in plate domains", *C. R. Méc.* **344** (2016), p. 225-235.
[20] Y. Jia, J. M. Bergheau, J. B. Leblond, J. Ch. Roux, R. Bouchaoui, S. Gallée, A. Brosse, "A new nodal-integration-based finite element method for the numerical simulation of welding processes", *Metals* **10** (2020), p. 1386-1403.
[21] O. C. Zienkiewicz, R. L. Taylor, J. Z. Zhu, in *The Finite Element Method: Its Basis and Fundamentals*, Butterworth-Heinemann, Oxford, 7th ed., 2013.
[22] M. A. Puso, J. Solberg, "A stabilized nodally integrated tetrahedral", *Int. J. Numer. Methods Eng.* **67** (2006), p. 841-867.
[23] M. A. Puso, J. S. Chen, E. Zywicz, W. Elmer, "Meshfree and finite element nodal integration method", *Int. J. Numer. Methods Eng.* **74** (2008), p. 416-446.
[24] SYSWELD™, *Reference Analysis Manual*, ESI Group, Rungis, France, released: 2020.
[25] C. Weissenfels, "Direct nodal imposition of surface loads using the divergence theorem", *Finite Elem. Anal. Des.* **165** (2019), p. 31-40.
[26] Y. Jia, J. B. Leblond, J. Ch. Roux, R. Lacroix, J. M. Bergheau, "Applications of a nodal-integration based finite element method to non-linear problems", in *14th WCCM and ECCOMAS Congress 2020 (Virtual Congress 2021)*, Scipedia, 2021.
[27] J. A. Goldak, M. J. Bibby, A. Chakravarti, "A new finite element model for welding heat sources", *Metall. Trans. B* **15** (1984), p. 299-305.